P2X7 receptor activity limits tumor infiltration by T cells

Andrea Romagnani[1†‡], Elsa Rottoli[1,2,‡], Emilia Maria Cristina Mazza[3†], Tanja Rezzonico-Jost[1], Benedetta De Ponte Conti[1,2], Michele Proietti[1,†], Michela Perotti[1,4], Elisa Civanelli[1,2], Lisa Perruzza[1], Alberico Luigi Catapano[5,6], Andrea Baragetti[5], Elena Tenedini[7], Enrico Tagliafico[7], Simonetta Falzoni[8], Francesco Di Virgilio[8], Giuseppe Danilo Norata[5], Silvio Bicciato[3] and Fabio Grassi[1,2,9,*]

[1]Institute for Research in Biomedicine, Faculty of Biomedical Sciences, Università della Svizzera Italiana, 6500 Bellinzona, Switzerland.
[2]Department of Medical Biotechnology and Translational Medicine, University of Milan, 20129 Milan, Italy.
[3]Department of Life Sciences, University of Modena and Reggio Emilia, 41125 Modena, Italy
[4]Institute for Microbiology, ETH Zürich, 8093 Zürich, Switzerland.
[5]Department of Excellence in Pharmacological and Biomolecular Sciences, University of Milan, 20133 Milan, Italy.
[6]IRCSS Multimedica, 20138 Milan, Italy.
[7]Department of Medical and Surgical Sciences for Children and Adults, University of Modena and Reggio Emilia, 41125 Modena, Italy.
[8]Department of Morphology, Surgery and Experimental Medicine, Section of Pathology, Oncology and Experimental Biology, University of Ferrara, 44121 Ferrara, Italy.
[9]Istituto Nazionale Genetica Molecolare "Romeo ed Enrica Invernizzi", 20122 Milan, Italy.

*Corresponding author. Email: fabio.grassi@irb.usi.ch
[‡]These authors contributed equally to this work
[†]Present address: F. Hoffmann-La Roche Ltd, 4070 Basel, Switzerland (A.R.); Laboratory of Translational Immunology, Humanitas Clinical and Research Center, 20089 Rozzano, Milan, Italy (E.M.C.M.); CCI-Center for Chronic Immunodeficiency, Universitätsklinikum Freiburg, 79106 Freiburg, Germany (M.P.).

Abstract

Extracellular adenosine triphosphate (eATP) is a signaling molecule, which variably affects directly or after hydrolysis to adenosine, all cells of the immune system. Whereas eATP is virtually absent in the interstitium of normal tissues, it can be present in the hundreds micromolar range in tumors, a concentration compatible with activation of the ATP-gated

ionotropic P2X7 receptor. Here we show that P2X7 activity in tumor-infiltrating T cells (TILs) induces cellular senescence and limits tumor suppression. P2X7 stimulation affects cell cycling of effector T cells and results in mitochondrial reactive oxygen species (ROS) generation and p38 MAPK dependent upregulation of *cyclin-dependent kinase inhibitor 1A* (*Cdkn1a*, encoding for p21$^{Waf1/Cip1}$). Lack of P2X7 promotes a transcriptional signature that correlates with enhanced cytotoxic T cell response in human solid tumors. In mice, transfer of tumor specific T cells with deletion of *P2rx7* significantly reduces tumor growth and extends survival, uncovering a purinergic checkpoint that can be targeted to improve the efficacy of cancer immunotherapy strategies.

Introduction

More than 30 years have passed since the first tumor infiltrating lymphocytes (TILs) were conditioned for treating patients with metastatic melanoma (1). Today, checkpoint inhibitors and chimeric antigen receptor (CAR) T cells have succeeded in promoting effective anti-tumor cytotoxicity with unprecedented durable responses in a variety of cancers, thereby establishing new immunotherapeutic paradigms for oncologic patients (2,3). Unfortunately, a substantial fraction of patients does not respond to current immunotherapy treatments. Thus, it has become important to identify factors that limit efficient T cell responsiveness in the tumor microenvironment, and to develop strategies that could potentially increase the patient response rates.

The tumor microenvironment can impair the effector functions of TILs by various mechanisms, including nutrients depletion (4,5) and release of immunosuppressive molecules, such as indoleamine 2,3-dioxygenase (IDO) (6), by cancer cells; recruitment of myeloid suppressor cells that release immunomodulators, such as arginase and nitrous oxide synthase (7); hypoxia (8) and

release of intracellular potassium ions by tumor-associated necrosis, both of which suppress T cell effector function (9). A characteristic feature of the tumor interstitium is the elevated concentration of extracellular ATP (eATP) (10), a pleiotropic signaling molecule, which can act as a danger-associated molecular pattern (DAMP). In fact, eATP contributes to adjuvant's efficacy in vaccination (11) and promotes immunogenic cell death of cancer cells by attracting antigen presenting cells and activating pro-inflammatory cascades (12); however, it can also limit pro-inflammatory T cell effector function (13) or generate immunosuppressive adenosine through the activity of plasma membrane ectonucleotidases (14). Therefore, the final effect of eATP in the tumor microenvironment would depend on the nature of the immune cell infiltrate, the composition of receptors for extracellular nucleotides and the activity of ATP-degrading ectonucleotidases.

Plasma membrane receptors for extracellular nucleotides, termed P2 receptors, are divided into two families, P2X and P2Y (15). P2X1 to P2X7 receptors are ATP gated non-selective cation channels, whereas P2Y receptors are guanine nucleotide–binding protein–coupled receptors (GPCRs), which bind also to ADP, UDP, UTP, or UDP-glucose. The P2X7 receptor is widely expressed with highest levels in the nervous and immune systems; it is characterized by dual gating that depends on the saturation level of the ligand binding sites. Activation of naïve P2X7 by low agonist concentrations results in slow desensitizing currents, whereas saturating or repetitive stimulations generate high-amplitude currents that lead to dilation of a pore permeable to nanometer-size dyes and eventually cell death (16,17). We found that P2X7 activity in TILs promotes cell cycle arrest, cellular senescence and impairs the tumoricidal response. Our results unravel P2X7 as a possible target to foster the adaptive T cell response against cancer cells in immunotherapeutic approaches.

Results

Enhanced anti-tumor response by *P2rx7*$^{-/-}$ CD8 T cells in lymphopenic mice

P2rx7 is the most expressed *P2rx* gene in both CD4^{+} T naïve and TEM cells (**Fig. S1A**). Nevertheless, real-time quantitative reverse transcription PCR (qRT-PCR) and western blot (WB) revealed significantly increased levels of *P2rx7* transcript and P2X7 protein, respectively, in TEM versus naïve cells (**Fig. S1, B and C**). The analysis of pore opening in flow cytometry in CD4^{+} T cells upon stimulation with the selective agonist 3'-*O*-(4-benzoyl) benzoyl ATP (BzATP) at 150 μM revealed that only a small fraction of naïve cells was sensitive to P2X7-mediated DAPI uptake, as compared to the vast majority of TEM cells (**Fig. S1D**), indicating enhanced sensitivity of CD4 cells to eATP after stimulation by cognate antigen and differentiation to effector/memory cells. An analogous upregulation of *P2rx7* transcripts was observed in CD8^{+} TEM cells (**Fig. S1E**).

In T cells, P2X7 stimulation can promote cell death by caspase-mediated gasdermin D processing and pyroptosis (13). In orthotopic human melanoma xenografts, eATP is present in the hundreds micromolar range (10,18). The analysis of B16 melanoma composed by cells stably expressing the eATP reporter pmeLUC (18) at day 7 after transplant into wild-type (WT) mice, revealed concentrations of eATP in the TME from tens to hundreds of micromolar (**Fig. S1F**).

We addressed whether P2X7 stimulation in the TME affected anti-tumor cytotoxicity of CD8^{+} TILs. The transfer of *P2rx7*$^{-/-}$ CD8^{+} naïve T cells into *Cd3ε*$^{-/-}$ mice that were subsequently engrafted with OVA expressing B16 (B16-OVA) melanoma cells (**Fig. 1A**) resulted in enhanced accumulation of *P2rx7*$^{-/-}$ TEM cells in the tumor but not in the spleen with respect to WT cells (**Fig. 1, B and C**). Tetramer staining revealed increased percentages of *P2rx7*$^{-/-}$ versus WT TILs specific for the H-2K^{b} restricted OVA peptide 257-264 (**Fig. 1D**). Moreover, tumor growth was

significantly delayed by *P2rx7*$^{-/-}$ with respect to WT cells (**Fig. 1E**).

Enhanced control of tumor growth and survival of mice by lack of P2X7 activity in tumor specific CD8 cells

Adoptive transfer of congenic *Rag1*$^{-/-}$/*P2rx7*$^{+/+}$ (OT-I) or *Rag1*$^{-/-}$/*P2rx7*$^{-/-}$ (OT-I *P2rx7*$^{-/-}$) OT-I TCR transgenic CD8^{+} cells specific for chicken ovalbumin peptide 257-264 presented by H2K^{b}, into WT mice bearing B16-OVA tumors (**Fig. 2A**), resulted in increased recoveries of tumor-infiltrating OT-I *P2rx7*$^{-/-}$ cells (**Fig. 2B**) that showed enhanced secretion of IFN-γ and Granzyme B with respect to OT-I cells (**Fig. 2C**). Since CD8^{+} OT-I naïve cells were primed *in vitro* before adoptive transfer into tumor bearing mice (19), we checked phosphatidylserine exposure and IFN-γ secretion before injection; no significant differences were detected between *P2rx7*$^{+/+}$ and *P2rx7*$^{-/-}$ cells (**Fig. S2, A and B**)**.** Moreover, since P2X7 activity can result in diminished recovery of particular T cell subsets during the *ex vivo* isolation procedure (20), we purified TILs in the presence of the selective P2X7 antagonist A-438079. We did not detect any difference in the percentages of OT-I or OT-I *P2rx7*$^{-/-}$ cells within CD8^{+} TILs irrespective of drug addition (**Fig. S2C**). In spite of the function of P2X7 in promoting caspase-mediated cell death (13), we found no difference in caspase activation between *P2rx7*$^{+/+}$ and *P2rx7*$^{-/-}$ TILs (**Fig. 2D**). However, *P2rx7*$^{-/-}$ cells proliferated more robustly than WT cells, as shown by staining with Ki-67 antibodies (**Fig. 2E**). Tumor infiltration by OT-I *P2rx7*$^{-/-}$ cells resulted in significant inhibition of tumor growth as compared to mice transferred with OT-I cells (**Fig. 2F**). Importantly, the transfer of OT-I *P2rx7*$^{-/-}$ cells promoted extended survival of mice (**Fig. 2G**), suggesting that P2X7 limits the expansion and tumoricidal activity of TILs. Consistent with enhanced capacity of OT-I *P2rx7*$^{-/-}$ cells to accumulate in the TME, co-transfer of OT-I and OT-I *P2rx7*$^{-/-}$ cells into

WT mice bearing B16-OVA tumors resulted in the significant dominance of OT-I *P2rx7*$^{-/-}$ TILs (**Fig. 2H**). Notably, OT-I *P2rx7*$^{-/-}$ cells were characterized by reduced expression of PD-1, which characterizes dysfunctional CD8 cells (**Fig. 2I**), whereas other checkpoint proteins, including Tim3 and CTLA4, were not differentially expressed by co-infiltrating *P2rx7*$^{+/+}$ and *P2rx7*$^{-/-}$ cells (**Fig. S2D**). These data suggest that lack of P2X7 endows TILs with improved resistance to dysfunctionality induced by the TME.

To substantiate these results within a different TME, we engrafted WT mice with OVA expressing MC-38 (MC38-OVA) colon adenocarcinoma cells and adoptively transferred OT-I or OT-I *P2rx7*$^{-/-}$ CD8^{+} cells (**Fig. 3A**). As observed in B16-OVA tumors, *P2rx7*$^{-/-}$ TILs were significantly increased with respect to *P2rx7*$^{+/+}$ cells (**Fig. 3B**) and expressed lower levels of PD-1 in the plasma membrane (**Fig. 3C**). Moreover, mice transferred with *P2rx7*$^{-/-}$ cells showed significantly reduced tumor growth and enhanced survival (**Fig. 3, D and E**), suggesting P2X7 deficient OT-I cells displayed enhanced anti-tumor functionality also in the MC-38 colon adenocarcinoma conditioned microenvironment.

Enhanced expansion of *P2rx7*$^{-/-}$ CD4 TEM cells in the TME

To address whether P2X7 activity could limit CD4^{+} T cells abundance in the tumor microenvironment, we adoptively transferred CD4^{+} naïve cells from WT or *P2rx7*$^{-/-}$ mice into *Cd3ε*$^{-/-}$ mice that were subsequently engrafted with B16 melanoma cells (**Fig. S3A**). Flow cytometry at 20 d after tumor transplant revealed a significant increase in *P2rx7*$^{-/-}$ with respect to WT TILs with TEM phenotype, but not in the spleen (**Fig. S3, B and C**). We did not detect differences in tumor growth between *Cd3ε*$^{-/-}$ mice either non-transferred or transferred with

P2rx7$^{-/-}$ or WT CD4^{+} naïve cells, consistent with lack of CD8^{+} T cell mediated cytotoxicity in *Cd3ε*$^{-/-}$ mice (**Fig. S3D**).

To mimic the effector response of CD4 cells to a tumor specific antigen in an immunocompetent organism, we adoptively transferred either *Rag1*$^{-/-}$/*P2rx7*$^{+/+}$ (OT-II) or *Rag1*$^{-/-}$/*P2rx7*$^{-/-}$ (OT-II *P2rx7*$^{-/-}$) congenic CD4^{+} OT-II TCR transgenic T cells specific for I-A^{b} restricted OVA peptide 323-339 into WT mice bearing B16-OVA tumors (**Fig. 4A**). As for *in vitro* primed CD8^{+} OT-I naïve cells, we checked phosphatidylserine exposure, and IFN-γ as well as IL-17 secretion before injection; no significant differences were detected between WT and *P2rx7*$^{-/-}$ cells (**Fig. S4, A and B).** In mouse naïve CD4 T cells, ADP-ribosylation of P2X7 by the ectoenzyme ADP-ribosyltransferase 2.2 (ARTC2.2) is responsible for nicotinamide adenine dinucleotide (NAD)-induced T cell death (NICD) (20). The analysis of OT-II T cells after *in vitro* activation and before injection into tumor bearing mice showed lack of ARTC2.2 expression, ruling out a possible function of ADP-rybosylation in impairing the expansion of WT with respect to *P2rx7*$^{-/-}$ cells (**Fig. S4C**). After 15 d, both OT-II and OT-II *P2rx7*$^{-/-}$ cells were barely detectable in the spleen (**Fig. S4D**), however OT-II *P2rx7*$^{-/-}$ cells were significantly increased in tumors as compared to OT-II cells (**Fig. 4B**). The percentage of Foxp3^{+} immunosuppressive T regulatory cells (Tregs) infiltrating the tumor tissue was not influenced by the expression of P2X7 in transferred *Rag1*$^{-/-}$ OT-II cells (**Fig. S4E**). Notably, tumor growth was significantly delayed in mice transferred with P2X7 deficient cells (**Fig. 4D**). The analysis of endogenous CD8^{+} TILs showed the significant increase of IFN-γ and TNF-α secreting cells in mice transferred with OT-II *P2rx7*$^{-/-}$ cells (**Fig. 4C**), suggesting lack of P2X7 fostered helper function to cytotoxic T cells that could contrast tumor growth more efficiently (21). Analogously to the results obtained with CD8 cells, co-transfer of OT-II and OT-II *P2rx7*$^{-/-}$ cells into WT mice bearing B16-OVA tumors

resulted in significant dominance of *P2rx7*$^{-/-}$ over *P2rx7*$^{+/+}$ cells (**Fig. 4E**), indicating that P2X7 deficient CD4 TEM cells are endowed with enhanced tumor infiltrating potential with respect to P2X7 proficient cells.

Regulated cell cycling in TEM cells by P2X7 activity

In CD4 naïve T cells, P2X receptors activation concomitantly to TCR stimulation contributes to productive T cell activation. In fact, P2X inhibition by the pharmacological antagonist periodate-oxidized ATP (oATP) in cells stimulated with anti-CD3/CD28 antibodies promotes T cell anergy (22). *P2rx7*$^{-/-}$ CD4 naïve cells did not show any difference in cell proliferation as compared to WT cells (**Fig. 5A**), suggesting that P2X1 and/or P2X4 could compensate for the lack of P2X7 activity, as observed in human T cells (23). In contrast, stimulation of *P2rx7*$^{-/-}$ TEM cells revealed a peculiar enhancement of cell proliferation with respect to the WT counterpart (**Fig. 5B**). To better address the contribution of P2X7 in regulating cell survival versus cycling, we applied a mathematical model to quantify division times and death rates within a time-course experiment in CD3/CD28 stimulated TEM cells (24). Graphical data extrapolation showed that *P2rx7*$^{-/-}$ TEM cells progressed earlier in the first cell division and required less time to enter subsequent cell divisions (**Fig. 5C**). At the same time, *P2rx7*$^{-/-}$ TEM cells were characterized by a reduced rate of cell death overtime as indicated by the slower exponential decay of the relative constant (**Fig. 5D**). These results indicate that *P2rx7*$^{-/-}$ TEM cells "perform" better than WT cells following TCR stimulation. To see whether an analogous difference could be detected following cytokine driven stimulation (without TCR engagement), we stimulated purified TEM cells with IL-2 or IL-7. In contrast to WT cells, which poorly proliferated, *P2rx7*$^{-/-}$ TEM cells effectively

expanded with both IL-2 and IL-7 (**Fig. 5, E and F**). Altogether, these data suggest that P2X7 activity limits TEM cell proliferation.

Transcriptional regulation of cell cycling by P2X7 in TEM but not naïve CD4 cell

To explore the transcriptional impact of *P2rx7* deletion in $CD4^+$ T naïve and TEM cells, we performed genome-wide expression profiling to compare *ex vivo* purified cells from WT and *P2rx7*$^{-/-}$ mice. Unsupervised analysis of gene expression levels showed that naïve cells grouped together independently from the genotype, while *P2rx7*$^{-/-}$ TEM cells were clearly separated from the WT counterpart, suggesting that *P2rx7* deletion substantially influences gene transcription in TEM but not naïve cells (**Fig. S5A**). Differential expression analysis resulted a transcriptional signature of 158 upregulated and 255 downregulated genes in *P2rx7*$^{-/-}$ TEM with respect to WT cells (FDR≤5% and absolute fold change≥1.5; **Table S1**) that discloses how *P2rx7* deficiency induces in TEM cells a transcriptional pattern intermediate between naïve and WT TEM cells (**Fig. S5B**). Functional over-representation analysis revealed that gene sets associated to DNA replication were enriched in *P2rx7*$^{-/-}$ TEM cells (**Fig. S5C**), whereas TCR/cytokine signaling, apoptosis and cell cycle arrest signatures were enriched in WT TEM cells (**Fig. S5D**). These results suggest that lack of P2X7 might confer greater proliferation potential to TEM cells in the eATP-rich tumor microenvironment. The efficacy of cytotoxic T cell response in human solid tumors has been associated to the magnitude of infiltrating $CD8^+$ cells expressing the integrin alpha E chain (CD103) together with the ATP-hydrolysing plasma membrane ectonucleoside triphosphate diphosphohydrolase-1 (CD39), suggesting that limiting P2X7 signaling in TILs could enhance the tumoricidal activity of these cells (25-27). Notably, genes over-expressed in *P2rx7*$^{-/-}$ TEM cells (**Table S2**) were significantly enriched in purified $CD103^{high}CD39^+$ TILs

(**Fig. S5E**) as well as in non-small-cell lung cancers (NSCLCs) and skin cutaneous melanoma (SKCM) transcriptomes from patients showing significantly improved survival (**Fig. S5, F and G**). These data suggest that diminished P2X7 activity could promote a transcriptional program, which more effectively controls tumor progression in humans.

Induction of T cell senescence by P2X7 activation

The genome-wide transcriptional analysis evidenced *Cdkn1a*, encoding for $p21^{Waf1/Cip1}$, as one of the most down-regulated transcript in *P2rx7*$^{-/-}$ TEM cells (**Fig. 6A, and Table S3**). *P2rx7* expression at different times after *in vitro* stimulation of naïve $CD4^+$ T cells directly correlated with *Cdkn1a*, suggesting signaling by P2X7 positively regulated *Cdkn1a* transcription (**Fig. 6B**). Accordingly, qRT-PCR on purified TEM cells stimulated with BzATP alone or together with A-438079 confirmed that signaling by P2X7 induced *Cdkn1a*; this induction was selective and did not affect *Cdkn1b* transcription (**Fig. 6C**). Coherently with gene array data and the function of P2X7 in regulating cell cycling activity, the transcription of *Trp53* and *Gadd45b* genes was also induced by BzATP (**Fig. 6D**). Moreover, addition of BzATP to *in vitro* stimulated WT $CD4^+$ TEM cells with anti-CD3/CD28 antibodies resulted in reduced Ki-67 staining and CellTrace Violet dilution, indicating inhibition of cell cycling activity. This effect was abrogated by A-438079 (**Fig. 6E**). BzATP showed a dose-dependent effect on cell proliferation that was observed also in $CD8^+$ WT TEM cells albeit with higher doses of BzATP (**Fig. S6, A and B**) and *Cdkn1a* was upregulated *in vitro* by BzATP (**Fig. S6C**). Notably, *Cdkn1a* transcript levels were significantly increased in WT as compared to *P2rx7*$^{-/-}$ $CD8^+$ TILs (**Fig. 6F**).

Cdkn1a is a well-characterized inhibitor of cell cycle progression and its activation by stress-induced p53 contributes to the onset of cellular senescence (28). To address whether P2X7

activity promoted TEM cells senescence, we stimulated *ex vivo* purified WT and *P2rx7*$^{-/-}$ TEM cells with anti-CD3/28 antibodies for 72h and analysed senescence-associated (SA) β-galactosidase (SA-β-gal). We observed reduced basal levels in *P2rx7*$^{-/-}$ cells and addition of BzATP to the culture of WT cells resulted in increase in SA-β-gal, suggesting P2X7 stimulation in TEM cells by eATP induces cellular senescence (**Fig. 7A**). Consistent with occurrence of the same phenomenon by P2X7 stimulation in effector T cells infiltrating the TME, SA-β-gal^{+} cells were significantly increased among OT-I with respect to OT-I *P2rx7*$^{-/-}$ TILs (**Fig. 7B**). P2X7 activity in T cells was associated with enhanced generation of mitochondrial ROS (29). MitoSOX staining of CD4 TEM cells showed an increase in mitochondrial ROS generation following BzATP stimulation and the frequency of *P2rx7*$^{-/-}$ cells stained with MitoSOX Red was significantly diminished with respect to WT cell, suggesting that lack of P2X7 resulted in reduced production of superoxide by mitochondria (**Fig. 7C**). ROS promote the formation of DNA damage foci that contain H2A.X histone phosphorylated at Ser139 (γH2A.X (30). Consistent with enhanced ROS production, WT TEM cells showed increased γH2A.X histone by P2X7 stimulation in Western blot that was inhibited by A-438079 (**Fig. 7D**). Cellular senescence in T cells can be actively maintained by p38 MAPK signaling (31). Stimulation of P2X7 induced p38 MAPK Thr180/Tyr182 phosphorylation (**Fig. 7E**), while pharmacological inhibition of p38 MAPK resulted in restoring basal levels of *Cdkn1a* transcripts (**Fig. 7F**). These results suggest that in the TME, P2X7 activation in TILs promotes cell cycle arrest and p38 MAPK mediated cellular senescence (**Fig. S7**).

Regulated cell cycling in human TEM cells by P2X7 activity

In humans, *P2RX7* gene polymorphisms generate functionally different P2X7 isoforms. We selected *P2rx7* SNP variants rs11065464 and rs1718119 encoding for hypo-functioning and hyper-functioning P2X7 receptors, respectively (32). Analogously to murine *P2rx7*$^{-/-}$ cells, human TEM cells bearing the hypomorphic P2X7 variant rs11065464 showed a significant decrease in the frequency of undivided cells after TCR stimulation compared to cells purified from subjects carrying the hyperactive rs1718119 SNP variant (**Fig. 8A**). The impaired progression in the cell cycle of these cells correlated with increased levels of *CDKN1A* transcripts (**Fig. 8A**). Knockdown of *P2RX7* in human CD4 or CD8 TEM cells (**Fig. S8A**) resulted in the reduction of undivided cells after TCR stimulation with concomitant reduction of *CDKN1A* expression (**Fig. 8, B and D**). The function of P2X7 in conditioning human TEM cells proliferation was confirmed by addition of BzATP during TCR stimulation that blocked cell cycle progression and upregulated *CDKN1A* (**Fig. 8, C and E, and Fig. S8B**). These results indicate that P2X7 activity limits the expansion potential of human TEM cells.

Discussion

T cells are potent effectors in controlling tumor growth and the extent of tumor infiltration by T cells has been generally considered a good prognostic marker in a number of tumor types (33). However, the peculiar nature of the TME results in a T cell response that is not proficient in controlling tumor growth. In melanoma patients, early effector T cells progress to a highly proliferating dysfunctional state (34). The composition of distinct dysfunctional $CD8^+$ subsets within TILs differentially influences the control of tumor growth and sensitivity to checkpoint blockade (35). Antigen recognition within the TME is hypothesized to be important in driving

the expansion of dysfunctional cells and in fact, elegant experiments in different tumors have shown that cytotoxicity is confined to non-tumor specific bystander cells that infiltrate the TME (36,37). In some cases, bystander cells dominated the pool of infiltrating CD8 cells, suggesting that the tumoricidal response would benefit from improving the quality of tumor-specific T cells (36). T cells transduced with chimeric antigen receptors (CARs) can mediate specific destruction of hematological malignancies and yield durable therapeutic responses (38). However, in solid tumors, the induction of a dysfunctional state and loss of T cell effector function by chronic antigen stimulation limit the efficacy of this immunotherapeutic approach (39-41). In this respect, NR4A transcription factors have been recently shown to contribute to the hyporesponsiveness of CAR T cells in experimental models of solid tumors (42).

The P2X7 receptor plays pleiotropic roles in shaping T cell function. In Tfh cells it triggers caspase activation and pyroptosis, a mechanism that limits the expansion of pathogenic CD4 cells in systemic lupus erythematosus (13). An analogous signaling is likely responsible of cell death induced by bacteria derived ATP in Tfh cells in the Peyer's patches of the small intestine to ensure controlled generation of T cell dependent secretory IgA and host-microbiota mutualism (43). Among downregulated genes between WT and *P2rx7*$^{-/-}$ TEM cells, we identified *erythroid differentiation regulator 1* (*Erdr1*), which encodes for a secreted protein that induce Fas-dependent T cell apoptosis, suggesting P2X7 activity can promote T cell death also by this signaling pathway (44). Importantly, acute TCR stimulation of Tfh cells robustly downregulates *P2rx7* expression, thus protecting antigen responding T cell from cell death (43). Similar results have been obtained in tissue resident memory T cells, suggesting that selective downregulation of *P2rx7* in T cells that productively respond to cognate antigen would ensure the amplification of pathogen-destructing cells during infections (45). In contrast, P2X7 activity is required for the

establishment and maintenance of long-lived central and tissue-resident memory CD8 T cells in mice, probably reflecting the function of P2X7 as ion channel in promoting mitochondrial function and metabolic fitness (46). Herein, we have shown that P2X7 stimulation in tumor-specific T cells within the TME results in stress-induced cellular senescence that limits the expansion of tumoricidal cells. We hypothesize targeting of P2X7 in effector TILs might provide a rejuvenating signal able to perpetuate the tumoricidal response.

It is important to consider that stimulation of P2X7 in cells of the innate immune system and/or cancer cells by eATP can contribute to T cell priming and control of tumor growth (12). Accordingly, tumor bearing P2X7 null mice showed lack of inflammatory infiltration and accelerated tumor progression (47). Nevertheless, an opposite outcome (i.e. enhanced control of tumor growth) with enhancement of pro-inflammatory TILs was observed by treating WT mice after tumor engrafting with a P2X7 selective antagonist (18). These data show how the eATP/P2X7 axis can dramatically influence tumor progression depending on the timing and cell types it activates. Our observations are important to discriminate the possible overall effect of P2X7 inhibition in the TME versus T cell selective P2X7 inhibition that could improve the tumoricidal potential of CAR T cells or TILs expanded *in vitro* in immunotherapeutic approaches.

Materials and Methods

Mice and *in vivo* experiments

All animal experiments were performed in accordance with the Swiss Federal Veterinary Office guidelines and authorized by the Cantonal Veterinary. C57BL/6J, *P2rx7*$^{-/-}$ (B6.129P2-*P2rx7*^{tm1Gab}/J), *Cd3ε*$^{-/-}$**,** OT-II *Rag1*$^{-/-}$ [B6.Cg-Tg(TcraTcrb)425Cbn/J], OT-I *Rag1*$^{-/-}$ [B6.Cg-

Tg(TcraTcrb)1100Mjb/DcrJ], CD45.1 (B6.SJL-Ptprca Pepcb/BoyJ) mice were bred in specific pathogen-free (spf) facility at the Institute for Research in Biomedicine, Switzerland. OT-II *Rag1*$^{-/-}$ *P2rx7*$^{-/-}$ and OT-I *Rag1*$^{-/-}$ *P2rx7*$^{-/-}$ were generated by crossing OT-II *Rag1*$^{-/-}$ or OT-I *Rag1*$^{-/-}$ with *P2rx7*$^{-/-}$ mice. Genotyping was accomplished by the polymerase chain reaction (PCR) method according to the manufacturer's protocol. Mice were housed, five per cage, in ventilated cages under standardized conditions (20 ± 2ºC, 55 ± 8% relative humidity, 12 h light/ dark cycle). Food and water were available ad libitum, and mice were examined daily. To analyze anti-tumor response, $CD4^+$ or $CD8^+$ T naïve were sorted from C57BL/6J and *P2rx7*$^{-/-}$ mice as described below. $2.5x10^5$ T naïve or TEM cells were injected into *Cd3ε*$^{-/-}$ mice. Melanoma B16 cells were harvested at exponential growth. After five days from transfer of T cells, melanoma cells were resuspended in PBS at a concentration of $5x10^6$ cells/mL and a volume of 0.1 mL ($5x10^5$ tumor cells) was injected subcutaneously into the back of adoptively transferred *Cd3ε*$^{-/-}$ mice. To analyse the T cell response against a tumor specific antigen, C57BL/6 or CD45.1 mice were injected subcutaneously with $5x10^5$ B16-OVA or MC38-OVA cells. After 5 or 7 days, $1x10^6$ *Rag1*$^{-/-}$ or *Rag1*$^{-/-}$/*P2rx7*$^{-/-}$ congenically marked $CD4^+$ OT-II or $CD8^+$ OT-I, that had been previously activated in vitro with anti-CD3 and anti-CD28 antibodies for 72h and IL-2 was in the last 24h prior to injection (19), were transferred into mice randomized from littermate cages and tumor growth was assessed. Tumor growth was scored with a caliper by measuring the greatest tumor diameter and its perpendicular to determine an average and then the area was calculated as: $(\text{average}/2)^2\pi$. Tumor-bearing animals were sacrificed after 20 days or earlier when showing any sign of discomfort. For analysis of survival, mice were sacrificed when they reached human endpoint, defined by: tumor volume [estimated with the formula (lengh x width^2)/2] bigger than 1,5 cm^3 or severe signs of discomfort.

Cell isolation from mice organs

For *in vitro* experiments and adoptive transfer, $CD4^+$ or $CD8^+$ T naïve, TEM or congenically marked OT-II or OT-I cells were sorted at FACSAria (BD Biosciences) from pooled cell suspensions of spleen, inguinal, axillary, brachial, cervical and mesenteric lymph nodes collected from C57BL/6J and *P2rx7*$^{-/-}$ mice. T naïve cells were sorted as $CD4^+$ or $CD8^+$, $CD62L^+$, $CD44^-$ and $CD25^-$ cells, TEM cells were sorted as $CD4^+$ or $CD8^+$, $CD62L^-$, $CD44^+$ and $CD25^-$ cells. OT-I and OT-II cells were sorted as $CD8^+$ and $CD4^+$, respectively, $CD25^-$ and $CD45.1^+$ or $CD45.1^-$ cells. Magnetic Cell Sorting (MACS, Miltenyi Biotec) with anti-CD4 and anti-APC mAbs were used to enrich cell subsets from complex cell mixtures.

Tumor cell lines

B16, B16-OVA, MC38OVA cells were cultured in RPMI-1640 supplemented with 10% heat-inactivate fetal bovine serum, 100 U/mL penicillin/streptomycin and 100 U/mL kanamycin. Cells were maintained in 5% CO_2 at 37°C. Tumor cells at 70-80% confluency were harvested by diluting them 1:5 in 0.25% trypsin.

Generation of stable B16F10-pmeLUC transfectants

B16F10 cells were transfected with Lipofectamine 2000 (Lifetechnologies, Monza, Italy). Selection was performed in the presence of G418 sulfate (0.2-0.8 mg/ml, Calbiochem), and single pmeLUC-transfected B16F10 clones were isolated by limiting dilution.

Luciferase and *in vivo* imaging

Luciferase luminescence was acquired with a total body luminometer (IVIS Lumina, Caliper-PerkinElmer). Mice were anesthetized with 2.5% isofluorane, intraperitoneally (i.p.) injected with 150 mg/kg D-luciferin (PerkinElmer), and luminescence quantified after 15 minutes.

Regions of interest (ROI) from displayed images were identified at tumour sites and quantified as Total Flux (photons/sec) using the Living Image software.

In vitro calibration of B16F10-pmeLUC cells

B16F10-pmeLUC cells, $1x10^5$ per well, plated in 24 wells plate, were incubated in RPMI 1640 medium and challenged with increasing concentration of ATP in the presence of D/luciferine, 60mg/ml. Luminescence was acquired with the IVIS luminometer for 1 min. Total luminescence emission was acquired from each well and quantified as Total Flux (photons/sec) using the Living Image software. Luminescence was expressed as Total Flux (photons/sec) as a function of the added ATP concentration.

Cell isolation from tumor tissue

Tumors were cut in small pieces and resuspended in RPMI-1640 with 1.5 mg/mL type I collagenase (Sigma), 100 μg/mL DNase I (Roche) and 5% FBS, digested for 45 min at 37°C under gentle agitation. The digestion product was then passed through a 70 μm cell strainer to obtain a single cell suspension. Lymphocytes were then enriched by Percoll density gradient following manufacturer's protocol.

Antibodies and flow cytometry

The following anti-mouse mAbs were purchased from eBioscience: APC conjugated anti-CD62L (clone: MEL-14, Cat.#: 17-0621-83), PE conjugated anti-Ki-67 (clone: SolA15, Cat.#: 12-5698-80), APC conjugated anti-CD27 (clone: LG.7F9, Cat.#: 17-0271-81), APC conjugated anti-CD8α (clone: 53-6.7 Cat.#: 17-0081-83), eFluor450 conjugated anti-Vα2 TCR(clone: B20.1, Cat.#: 48-5812-80). The following mAbs were purchased from BioLegend: PE conjugated anti-CD44 (clone: IM7, Cat.#: 103008), PE/Cy7 conjugated anti-CD25 (clone: OC61, Cat.# 102016), APC/Cy7 conjugated anti-CD4 (clone: RM4-5, Cat.#: 100526), PE/Cy7 conjugated anti-CD3

(clone: 145-2C11, Cat.#: 100320), Pacific Blue conjugated anti-CD8α (clone: 53-6.7, Cat.#: 100725), FITC conjugated anti-TCRβ (clone: H57-597, Cat.# 109215), APC conjugated anti-CD8α (clone: 53-6.7, Cat.# 17-0081-83), PE/Cy7 conjugated anti-CD45.1 (clone: A20, Cat.#: 2020-01-31), APC/Cy7 conjugated anti-mCD90.2 (clone: 30-H12, Cat#: 105328), PE conjugated anti-CTLA-4 (clone: UC10-4B9, Cat.#: 106305), APC conjugated anti-Tim3 (clone: B8.2C12, Cat.#: 134007), PercP/Cy5.5 conjugated anti-PD1 (clone: RMPI-30, Cat.#: 109120). The following mAb was purchased from BD Bioscience: PE conjugated anti-Vβ 5.1, 5.2 TCR (clone:F23.1 Cat#: BDB553862). Intracellular staining was performed using the BD Cytofix/Cytoperm and Perm/Wash buffers or, for intracellular FoxP3 (APC, clone: FJK-16s; eBioscience Cat.#: 17-5773-82) staining, the eBioscience FoxP3 staining buffer set. For intracellular staining of IFN-γ (PE-labeled, clone: XMG1.2; Biolegend Cat.#: 505808) TNF-α (APC-labeled, clone: MP6-XT22; eBioscience Cat.#: 506308), IL-17 (PercP/Cy5 labeled, clone: eBio17B7 cat.#: 45-7177-82) T cells were incubated for 4 h at 37 °C in ionomycin (750 ng/ml) and PMA (20ng/ml). For the last 3 h, Brefeldin (eBioscience, 1000X Solution) was added to the cultures. For tetramer staining cells were labelled for 2 h at 37 °C with H-2K^{b} OVA Tetramer SIINFEKL-PE (MBL, iTAg MHC tetramer, Cat. #: T0300). Activated caspases were quantified using Vybrant® FAM Poly Caspases Assay Kit (Invitrogen, Cat.#: V35117), according to the manufacturer's protocol.

The following anti-human proteins mAbs were purchased from Life Technologies: PE-Texas Red conjugated anti-CD4 (clone: S3.5, Cat.# MHCD0417), QD655 conjugated anti-CD45RA (clone: MEM-56, Cat#. Q10069). The following mAbs were purchased from BioLegend: PE conjugated anti-CCR7 (clone: G043H7, Cat#. 353204), PE/Cy5 conjugated anti-CD25 (clone: BC96, Cat.#: 302608). FITC conjugated anti-CD8 (clone: B9.11, Cat.#: A07756). Samples were

acquired on a LSRFortessa (BD Bioscience) flow cytometer. Data were analyzed using FlowJo software (TreeStar) or FACS Diva software (BD Bioscience).

Real-time quantitative reverse transcription PCR (qRT-PCR)

Total RNA from FACS sorted cells was precipitated in Trizol (Invitrogen) and reverse transcribed to cDNA using Random hexamers (Roche, Cat.#: R 15504) and M-MLV reverse-transcriptase (Invitrogen, Cat.#: 28025-013) following manufacturer's protocol. mRNA samples were treated with 2 U/sample of DNase (Applied Biosystems). Transcripts were quantified by real-time PCR on an ABI PRISM 7700 Sequence Detector with predesigned TaqMan Gene Expression Assays and reagents according to the manufacturer's instructions (https://www.lifetechnologies.com). The following probes were used for mouse cells: *Cdkn1a* (Mm00432448_m1), *Cdkn1b* (Mm00432448_m1), *P2rx1* (Mm00435460_m1), *P2rx2* (Mm01202368_g1), *P2rx3* (Mm00523699_m1), *P2rx4* (Mm00501787_m1), *P2rx5* (Mm00473677_m1), *P2rx6* (Mm00440591_m1), *P2rx7* (Mm01199500_m1), *Trp53* (Mm01731290_g1), *Gadd45b* (Mm00435123_m1). The following probes were used for human cells: *CDKN1A* (Hs00355782_m1), *P2RX7* (Hs00175721_m1). All reactions were performed in triplicate. The relative amounts of mRNAs were calculated by the ΔCT method. *Hprt* for mouse cells and *TBP* for human cells were used as internal housekeeping genes.

Time monitoring of DAPI uptake

Purified T naïve or TEM cells were resuspended at $1x10^6$ cells/mL and loaded with DAPI (1 µg/mL). After 30 seconds of measurement for DAPI basal level, cells were stimulated with BzATP and DAPI uptake was monitored over time (250 seconds) at LSRFortessa and the kinetics analyzed using FlowJo software.

Gene expression profiling of *ex vivo* purified $CD4^+$ cells

Gene expression profiling of *ex vivo* purified $CD4^+$ cells was performed on MG-430 PM Array Strip (Affymetrix, Santa Clara, CA, USA). Briefly, total RNA was extracted using TriPure (Roche) from *ex vivo* purified $CD4^+$ naïve and TEM cells from WT (*n*=2 and *n*=3 independent samples for naïve and TEM, respectively) and *P2rx7*$^{-/-}$ (*n*=2 and *n*=3 independent samples for naïve and TEM, respectively) mice. RNA quality and purity were assessed on the Agilent Bioanalyzer 2100 (Agilent Technologies, Waldbronn, Germany); RNA concentration was determined using the NanoDrop ND-1000 Spectrophotometer (NanoDrop Technologies Inc.). In vitro transcription, hybridization and biotin labeling were performed according to Affymetrix GeneChip 3'IVT protocol and processed using GeneAtlas™ Platform (Affymetrix, Santa Clara, CA, USA). Scanning and data exporting was performed using standard Affimetrix protocols. All microarray data analyses were performed in R (version 3.3.2) using Bioconductor libraries (BioC 3.1) and R statistical packages. Probe level signals were converted to expression values using robust multi-array average procedure RMA (48) of Bioconductor *affy* package and a custom definition file for mouse HT array plates based on Entrez genes from BrainArray (version 22.0.0; http://brainarray.mbni.med.umich.edu/Brainarray/Database/CustomCDF/22.0.0/entrezg.asp). Raw data are available at Gene Expression Omnibus under accession number GSE118146.

To identify genes associated with *P2rx7* deletion in *ex vivo* purified $CD4^+$ TEM cells, we compared the expression levels of WT and *P2rx7*$^{-/-}$ TEM cells using the Significance Analysis of Microarray (SAM) (49) algorithm coded in the *samr* R package. In SAM, we estimated the percentage of false positive predictions (i.e. False Discovery Rate, FDR) with 100 permutations and selected those probe sets with FDR $\leq$ 5% and absolute fold change larger than a selected

threshold (e.g. ≥ 1.5) in the comparison of TEM cells from *P2rx7*$^{-/-}$ and WT mice (tables S1 and S3).

Global unsupervised and supervised clusterings were performed using the function *hclust* of R *stats* package with Pearson correlation as distance metric and average agglomeration method. Gene expression heatmaps have been generated using the function *heatmap.2* of R *gplots* package after row-wise standardization of the expression values. Before unsupervised clustering, to reduce the effect of noise from non-varying genes, we removed those probe sets with a coefficient of variation smaller than the 95th percentile of the coefficients of variation in the entire dataset. The filter retained 904 genes that are more variable across samples in any of the 4 subsets (naïve and TEM cells from *P2rx7*$^{-/-}$ and WT mice).

The volcano plot, showing the most significantly differentially expressed genes in the comparison of ex vivo purified CD4+ TEM cells from P2rx7$^{-/-}$ and WT mice, was generated using the *ggplot* function of the *ggplot2* R package. P-values were derived from SAM q-values using the function *samr.pvalues.from.perms* of the *samr* R package (table S3).

Functional over-representation was performed using Gene Set Enrichment Analysis (GSEA; http://software.broadinstitute.org/gsea/index.jsp) and the curated gene sets of the Molecular Signatures Database (MSigDB) derived from the KEGG pathway database (http://software.broadinstitute.org/gsea/msigdb/genesets.jsp?collection=CP:KEGG). GSEA was applied on log2 expression data of *P2rx7*$^{-/-}$ and WT TEM cells. Prior to GSEA analysis, we converted mouse Entrez IDs into the corresponding human homologous genes using the HUGO Gene Nomenclature Committee (HGNC) database (https://www.genenames.org/cgi-bin/hcop). Gene sets were considered significantly enriched at FDR≤0.25 when using Signal2Noise as metric and 1,000 permutations of gene sets.

Gene expression data that support the findings of our study have been deposited in NCBI Gene Expression Omnibus (GEO) and are accessible through the link:

https://www.ncbi.nlm.nih.gov/geo/query/acc.cgi?acc=GSE118146

by using the following secure token: oxmpkqkotfidbuz.

Collections of cancer transcriptomes

Bulk RNA-seq data of purified populations of $CD8^+$ T cells isolated from primary lung tumors were derived from ref. 26. Transcriptional data were downloaded from the series matrix file of GSE90728 and used as are. The status of CD103 (ITGAE) gene in NSCLC $CD8^+$ TILs was derived from table S1 of ref. 26. The expression level of the *P2rx7*$^{-/-}$ up-regulation signature (FDR≤5% and fold change≥1.5; see table S2) has been calculated as the standardized average expression of all *P2rx7*$^{-/-}$ up-regulated genes in $CD103^{low}CD39^-$, $CD103^{intermediate}$, and $CD103^{high}CD39^+$ TIL subgroups.

To identify groups of tumors with either high or low *P2rx7*$^{-/-}$ up-regulation signature, we used the classifier described in Adorno et al. (50), that is a classification rule based on a signature score obtained summarizing the standardized expression levels of signature genes into a combined score with zero mean. Tumors were classified as *P2rx7*$^{-/-}$ up-regulation signature "low" if the combined score was negative and as *P2rx7*$^{-/-}$ up-regulation signature "high" if the combined score was positive. This classification was applied to expression values of a non-small-cell lung cancer (NSCLC) compendium and of the TCGA skin cutaneous melanoma (SKCM) dataset. The NSCLC compendium has been created from 7 major datasets comprising microarray data of lung cancer samples annotated with clinical outcome. All data were measured on Affymetrix arrays and have been downloaded from NCBI Gene Expression Omnibus GSE3141, GSE10245, GSE14814, GSE19188, GSE31210, and GSE68465 and from the Ladanyi

and Gerald Laboratories Lung Adenocarcinoma microarray repository (http://cbio.mskcc.org/public/lung_array_data/). Prior to analysis, we eliminated duplicate samples and renamed all original sets after the medical center where patients were recruited. This re-organization returned 1,136 unique samples from 10 independent cohorts comprising 989 adenocarcinomas (778 of which with complete clinical outcome information) and 147 squamous cell carcinomas. The type and content of clinical and pathological annotations of the compendium samples have been derived from the original cohorts. Since raw data (.CEL files) were available for all samples, the integration, normalization and summarization of gene expression signals has been obtained applying the procedure described in Rustighi et al (51). Briefly, expression values were generated from intensity signals using a custom CDF obtained merging HG-U133A, HG-U133A2 and HG-U133 Plus2 original CDFs and transforming the original CEL files accordingly. Intensity values for a total of 21,995 probe sets have been background-adjusted, normalized using quantile normalization, and gene expression levels calculated using median polish summarization (multi-array average procedure, RMA). Clinical information among the various datasets has been standardized as described in Cordenonsi et al (52). Gene expression data (raw counts) and clinical information of the TCGA skin cutaneous melanoma (SKCM) dataset were downloaded from the Genomic Data Commons Portal using functions of the *TCGAbiolinks* R package. Raw counts were normalized and gene expression levels quantified as counts per million (cpm) using functions of the *edgeR* R package. To evaluate the prognostic value of the *P2rx7*$^{-/-}$ up-regulation signature, we estimated, using the Kaplan– Meier method, the probability that patients would remain metastasis-free or alive. To confirm these findings, the Kaplan–Meier curves were compared using the log-rank (Mantel–

Cox) test. P-values were calculated according to the standard normal asymptotic distribution. Survival analysis was performed in GraphPad Prism.

***In vitro* monitoring of cell survival and proliferation**

T naïve or TEM cells were grown in a 96 flat-bottom well plate in RPM-1640 supplemented with 10% heat-inactivated fetal bovine serum, 100 U/mL penicillin/streptomycin and 100 U/mL kanamycin and maintained in 5% CO_2 at 37°C. Cells were labeled with CellTrace violet (Thermo Fisher, Cat.#: C34557) and stimulated by plate-bound anti-CD3ε mAb (2μg/mL) with co-immobilized anti-CD28 mAb (2μg/mL) (eBioscience); for stimulation with cytokines, cells were cultured with IL-2 at 50 U/mL. CellTrace dilution was measured in viable cells through the exclusion of dead and apoptotic cells by electronically gating PI and Annexin V negative cells. FACS acquisitions were standardized by fixed numbers of calibration beads (BD Biosciences). Half-life and cell cycling activity was calculated as previously described (24).

Quantification of β-galactosidase and mitochondria-associated ROS

To measure cellular senescence, purified TEM cells were stimulated for 3 days with anti-CD3 and CD28 mAbs in the presence or absence of 70 μM BzATP. The following protocol was used also for OT-I cells were collected from tumors. Cells were incubated for 2 h with 100 nM bafilomycin A1 to inhibit lysosomal β-galactosidase before adding the β-galactosidase substrate C_{12}FDG (Thermo Fisher). Relative β-galactosidase activity was assessed as fluorescence emission at FACS (with 488 nm laser). Mitochondria-associated ROS levels were measured by staining cells with MitoSOX red (Molecular Probes/Invitrogen) at 5 μM for 40 min at 37ºC. Cells were then washed and resuspended in PBS for FACS analysis (with laser for PE).

Western blotting

For western blot analysis TEM cells were washed with ice cold PBS and lysed with RIPA buffer 1x (Sigma) or with Urea 9 M to detect nuclear protein, both supplemented with phosphatase inhibitor cocktail (Sigma-Aldrich) and protease inhibitor cocktail (Roche). Samples were centrifuged at 14.000 rpm for 10 min at 4°C and snap frozen. Cleared protein lysate was denatured with loading buffer supplemented with DTT 0.1 μM for 10 min at 65°C. Samples were run on precast 4-12% bis-tris protein gels (BioRad) and then transferred onto PVDF membranes using Trans-Blot Turbo Transfer System (BioRad). Membranes were blocked with 10% (wt/vol) nonfat dry milk (Bio-Rad) and 0.1% Tween-20 in TBS and incubated with appropriate antibodies in TBS with 0.1% Tween-20 for 16 h at 4 °C. The following antibodies were purchased from Cell Signaling Technology: anti-p38 MAPK (rabbit, Cat. #9212), anti-phospho p38MAPK (T180/Y182) (rabbit, clone: D3F9, Cat. #4511), anti-phospho H2A.X (S139) (rabbit, clone: 20E3, Cat. #9718), anti-p21 (rabbit, clone 12D1 Cat.#2947) and anti-Vinculin (rabbit, clone:E1E9V Cat.#:13901). Anti-GAPDH antibody (mouse, clone: 6C5 Cat. #MAB374) was purchased from Millipore. All incubations with primary antibody were followed by incubation with secondary HRP-conjugated anti-rabbit (Cat. #7074, Cell Signaling Technology), or anti-mouse (Cat. #7076, Cell Signaling Technology) IgG antibodies in TBS with 0.1% Tween-20. Membranes were developed using the Pierce ECL Western blotting substrate (Thermo Scientific, Cat.# 32209), signals were detected with the ImageQuant LAS 4000 system in the standard acquisition mode (GE Healthcare Life Sciences), and bands were quantified using the Multi Gauge Analysis tool (Fujifilm).

Identification of human SNP variants, TEM cells isolation and transfection

The Progressione della Lesione Intimale Carotidea (PLIC) Study (a sub-study of the CHECK study) is a large survey of the general population of the northern area of Milan (n= 2.606) (53,54), followed at the Center for the Study of Atherosclerosis, Bassini Hospital (Cinisello Balsamo, Milan, Italy). The Study was approved by the Scientific Committee of the Università degli Studi di Milano ("Cholesterol and Health: Education, Control and Knowledge – Studio CHECK (SEFAP/Pr.0003) – reference number Fa-04-Feb-01) in February 4th 2001. An informed consent was obtained by subjects in accordance with the Declaration of Helsinki. Within the PLIC Cohort, 2,274 subjects were genotyped for two variants in the *P2RX7* locus: a) the rs11065464, g.36458C>A intron variant, associated with loss-of-function P2X7 pore forming (55) and the rs1718119 Ala228Thr missense variant, determining increase in receptor activity (55). Both variants were not in linkage disequilibrium and their respective minor allele frequencies were in accordance to the Hardy-Weinberg equilibrium. For the first variant, out of 2,274, we found 1,183 homozygous wild-type (CC), 907 heterozygous (CA) and 184 mutated form (AA) homozygous carriers. For the missense variant, out of 2,274, we found 1,008 homozygous wild-type (CC), 1,011 heterozygous (CA) and 255 mutated form (AA) homozygous carriers. Genomic DNA was extracted using Flexigene DNA kit (Qiagen, Milan ,Italy) and the genotyping was performed by quantitative real time PCR as previously described (56).

The permission to perform the experiments is authorized according to the Swiss law by the Federal Office for the Environment (FOEN) under the notification number A080059. Peripheral blood mononuclear cells (PBMCs) were isolated from blood by density-gradient centrifugation using Ficoll-Paque™ Plus gradient (GE-Healthcare). $CD4^+$ and $CD8^+$ T cells were enriched using human anti-CD4 or anti-FITC MicroBeads (Miltenyi Biotec) and then $CD4^+$ and $CD8^+$ TEM cells were sorted with a FACSAria (BD) as $CD4^{+/-}$, $CD8^{+/-}$, $CCR7^-$, $CD45RA^-$ and $CD25^-$.

To knock-down *P2RX7* gene, TEM cells were electroporated with Neon transfection kit and device (Invitrogen). A total of $5x10^5$ TEM cells were washed three times with PBS and resuspended in 10 µL of Buffer T (Neon kit, Invitrogen). 40 pmol of *P2RX7* Silencer Select Pre-designed siRNA (Ambion) or, as a control, siGLO Green Transfection Indicator (Dharmacon) were added to the cells to a final volume of 11 µL and mixed. 10 µL of the suspension was electroporated with Neon electroporation Device (Invitrogen; 2150 V, 30 ms, 1 pulse). Electroporated cells were then transferred in RPMI-1640 supplemented with 10% FBS and without antibiotics for 24 hours. For analysis of cell proliferation, electroporated TEM cells were labelled with CellTrace violet (Thermo Fisher, Cat.#: C34557) and plated on 96 well NUNC immunoplate coated with anti-CD3 (5 µg) and anti-CD28 (1 µg) antibodies for 5 days.

Statistical analyses

Statistical analysis was performed with the Prism software (GraphPad). Comparisons of two groups were calculated using nonparametric Mann Whitney test or Student's unpaired t test. Comparisons for more than two groups were calculated using Kruskall-Wallis test followed by Dunn's multiple comparison test. Results are presented as mean values ± SEM. Values of $P<0.05$ were considered significant.

Supplementary Materials

Fig. S1. *P2rx7* expression and function in murine T cells and eATP *in vivo* measurement.

Fig. S2. Characterization of OT-I cells before injection, *ex vivo* recovery, and CTLA-4 and TIM-3 expression in OT-I TILs.

Fig. S3. P2X7 activity limits amplification of homeostatically expanded $CD4^+$ T naïve cells in B16 melanoma.

Fig. S4. Characterization of OT-II cells before injection, ART2.2 staining of OT-I and OT-II cells before injection, recovery of OT-II cells from spleen and Treg cells from tumors.

Fig. S5. Genome-wide expression profiling of *ex vivo* purified $CD4^+$ naïve and TEM cells from WT and *P2rx7*$^{-/-}$ mice and enrichment of *P2rx7*$^{-/-}$ over-expressed genes in tumor samples.

Fig. S6. P2X7 mediated inhibition of TEM cell proliferation and induction of *Cdkn1a* in $CD8^+$ TEM cells.

Fig. S7. Model of P2X7 signaling in TILs.

Fig. S8. Knock-down of *P2RX7* by siRNA and western blot for $p21^{Waf1/Cip1}$ in human TEM cells.

Table S1. Differentially expressed genes between *P2rx7*$^{-/-}$ vs WT (q-value % <5 and absolute fold change >1.5)

Table S2. List of up-regulated genes in *P2rx7*$^{-/-}$ vs WT (q-value % <5 and absolute fold change >1.5) used in the analysis of GSE90728 lung data, NSCLC compendium and TCGA SKCM.

Table S3. Differentially expressed genes between *P2rx7*$^{-/-}$ vs WT (q-value % <5 and absolute fold change >2)

Author contributions

F.G., A.R. and E.R. designed experiments and analysed data. A.R., E.R., T.R-J., B.D.P.C., M.Pr., M.Pe., E.C., L.P., S.F. and F.D.V. performed experiments and analysed data. E.Te. and E.Ta. performed gene expression profiling. E.M.C.M. and S.B. conducted all the bioinformatics analyses. A.L.C, A.B. and G.D.N. screened and provided samples from the PLIC study. F.G. coordinated the study and wrote the manuscript.

Acknowledgments

We thank Sara Maffei (Institute for Research in Biomedicine, Bellinzona) for help with mice experiments, the NIH Tetramer Core Facility for providing tetramers. The work was supported by grant KFS–4110-02-2017-R of the Swiss Cancer Research, 310030_159491 and IZCNZ0-174704 of the Swiss National Science Foundation (to F.G.), AIRC Special Program Molecular Clinical Oncology ‘5 per mille’ grant 10016 and Italian Ministry of Education, University and Research and the National Research Council grant Italian Epigenomics Flagship Project (Epigen) (to S.B.). The work of the PLIC study was supported by grants 2015-0524 and 2015-0564 (to A.L.C.) and 2016-0852 (to G.D.N.) of Fondazione Cariplo, Italy; H2020 REPROGRAM PHC-03-2015/667837-2 (to A.L.C.); GR-2011-02346974 of Ministry of Health, Italy (to G.D.N.). The authors declare non-competing financial interests.

References

1. Rosenberg SA, Packard BS, Aebersold PM, Solomon D, Topalian SL, Toy ST*, et al.* Use of tumor-infiltrating lymphocytes and interleukin-2 in the immunotherapy of patients with metastatic melanoma. A preliminary report. The New England journal of medicine **1988**;319:1676-80
2. Paucek RD, Baltimore D, Li G. The Cellular Immunotherapy Revolution: Arming the Immune System for Precision Therapy. Trends in immunology **2019**;40:292-309
3. Topalian SL, Wolchok JD, Chan TA, Mellman I, Palucka K, Banchereau J*, et al.* Immunotherapy: The path to win the war on cancer? Cell **2015**;161:185-6
4. Chang CH, Qiu J, O'Sullivan D, Buck MD, Noguchi T, Curtis JD*, et al.* Metabolic Competition in the Tumor Microenvironment Is a Driver of Cancer Progression. Cell **2015**;162:1229-41

5. Ho PC, Bihuniak JD, Macintyre AN, Staron M, Liu X, Amezquita R*, et al.* Phosphoenolpyruvate Is a Metabolic Checkpoint of Anti-tumor T Cell Responses. Cell **2015**;162:1217-28
6. Munn DH, Mellor AL. IDO and tolerance to tumors. Trends in molecular medicine **2004**;10:15-8
7. Marigo I, Dolcetti L, Serafini P, Zanovello P, Bronte V. Tumor-induced tolerance and immune suppression by myeloid derived suppressor cells. Immunological reviews **2008**;222:162-79
8. Sitkovsky M, Lukashev D. Regulation of immune cells by local-tissue oxygen tension: HIF1 alpha and adenosine receptors. Nature reviews Immunology **2005**;5:712-21
9. Eil R, Vodnala SK, Clever D, Klebanoff CA, Sukumar M, Pan JH*, et al.* Ionic immune suppression within the tumour microenvironment limits T cell effector function. Nature **2016**;537:539-43
10. Pellegatti P, Raffaghello L, Bianchi G, Piccardi F, Pistoia V, Di Virgilio F. Increased level of extracellular ATP at tumor sites: in vivo imaging with plasma membrane luciferase. PloS one **2008**;3:e2599
11. Vono M, Taccone M, Caccin P, Gallotta M, Donvito G, Falzoni S*, et al.* The adjuvant MF59 induces ATP release from muscle that potentiates response to vaccination. Proc Natl Acad Sci U S A **2013**;110:21095-100
12. Kepp O, Loos F, Liu P, Kroemer G. Extracellular nucleosides and nucleotides as immunomodulators. Immunol Rev **2017**;280:83-92
13. Faliti CE, Gualtierotti R, Rottoli E, Gerosa M, Perruzza L, Romagnani A*, et al.* P2X7 receptor restrains pathogenic Tfh cell generation in systemic lupus erythematosus. The Journal of experimental medicine **2019**
14. Hatfield SM, Sitkovsky M. A2A adenosine receptor antagonists to weaken the hypoxia-HIF-1alpha driven immunosuppression and improve immunotherapies of cancer. Current opinion in pharmacology **2016**;29:90-6
15. Burnstock G. Purinergic signalling--an overview. Novartis Found Symp **2006**;276:26-48; discussion -57, 275-81
16. Browne LE, Compan V, Bragg L, North RA. P2X7 receptor channels allow direct permeation of nanometer-sized dyes. The Journal of neuroscience : the official journal of the Society for Neuroscience **2013**;33:3557-66
17. Khadra A, Tomic M, Yan Z, Zemkova H, Sherman A, Stojilkovic SS. Dual gating mechanism and function of P2X7 receptor channels. Biophysical journal **2013**;104:2612-21
18. De Marchi E, Orioli E, Pegoraro A, Sangaletti S, Portararo P, Curti A*, et al.* The P2X7 receptor modulates immune cells infiltration, ectonucleotidases expression and extracellular ATP levels in the tumor microenvironment. Oncogene **2019**
19. Klein Geltink RI, O'Sullivan D, Corrado M, Bremser A, Buck MD, Buescher JM*, et al.* Mitochondrial Priming by CD28. Cell **2017**;171:385-97 e11
20. Adriouch S, Hubert S, Pechberty S, Koch-Nolte F, Haag F, Seman M. NAD+ released during inflammation participates in T cell homeostasis by inducing ART2-mediated death of naive T cells in vivo. Journal of immunology **2007**;179:186-94
21. Borst J, Ahrends T, Babala N, Melief CJM, Kastenmuller W. CD4(+) T cell help in cancer immunology and immunotherapy. Nature reviews Immunology **2018**
22. Schenk U, Westendorf AM, Radaelli E, Casati A, Ferro M, Fumagalli M*, et al.* Purinergic control of T cell activation by ATP released through pannexin-1 hemichannels. Sci Signal **2008**;1:ra6
23. Woehrle T, Yip L, Elkhal A, Sumi Y, Chen Y, Yao Y*, et al.* Pannexin-1 hemichannel-mediated ATP release together with P2X1 and P2X4 receptors regulate T-cell activation at the immune synapse. Blood **2010**;116:3475-84
24. Hawkins ED, Hommel M, Turner ML, Battye FL, Markham JF, Hodgkin PD. Measuring lymphocyte proliferation, survival and differentiation using CFSE time-series data. Nature protocols **2007**;2:2057-67
25. Duhen T, Duhen R, Montler R, Moses J, Moudgil T, de Miranda NF*, et al.* Co-expression of CD39 and CD103 identifies tumor-reactive CD8 T cells in human solid tumors. Nature communications **2018**;9:2724
26. Ganesan AP, Clarke J, Wood O, Garrido-Martin EM, Chee SJ, Mellows T*, et al.* Tissue-resident memory features are linked to the magnitude of cytotoxic T cell responses in human lung cancer. Nature immunology **2017**;18:940-50
27. Savas P, Virassamy B, Ye C, Salim A, Mintoff CP, Caramia F*, et al.* Single-cell profiling of breast cancer T cells reveals a tissue-resident memory subset associated with improved prognosis. Nature medicine **2018**;24:986-93
28. Krenning L, Feringa FM, Shaltiel IA, van den Berg J, Medema RH. Transient activation of p53 in G2 phase is sufficient to induce senescence. Molecular cell **2014**;55:59-72

29. Foster JG, Carter E, Kilty I, MacKenzie AB, Ward SG. Mitochondrial superoxide generation enhances P2X7R-mediated loss of cell surface CD62L on naive human CD4+ T lymphocytes. Journal of immunology **2013**;190:1551-9
30. Rogakou EP, Pilch DR, Orr AH, Ivanova VS, Bonner WM. DNA double-stranded breaks induce histone H2AX phosphorylation on serine 139. The Journal of biological chemistry **1998**;273:5858-68
31. Akbar AN, Henson SM, Lanna A. Senescence of T Lymphocytes: Implications for Enhancing Human Immunity. Trends in immunology **2016**;37:866-76
32. Stokes L, Fuller SJ, Sluyter R, Skarratt KK, Gu BJ, Wiley JS. Two haplotypes of the P2X(7) receptor containing the Ala-348 to Thr polymorphism exhibit a gain-of-function effect and enhanced interleukin-1beta secretion. FASEB journal : official publication of the Federation of American Societies for Experimental Biology **2010**;24:2916-27
33. Motz GT, Coukos G. Deciphering and reversing tumor immune suppression. Immunity **2013**;39:61-73
34. Li H, van der Leun AM, Yofe I, Lubling Y, Gelbard-Solodkin D, van Akkooi ACJ*, et al.* Dysfunctional CD8 T Cells Form a Proliferative, Dynamically Regulated Compartment within Human Melanoma. Cell **2019**;176:775-89 e18
35. Miller BC, Sen DR, Al Abosy R, Bi K, Virkud YV, LaFleur MW*, et al.* Subsets of exhausted CD8(+) T cells differentially mediate tumor control and respond to checkpoint blockade. Nature immunology **2019**;20:326-36
36. Scheper W, Kelderman S, Fanchi LF, Linnemann C, Bendle G, de Rooij MAJ*, et al.* Low and variable tumor reactivity of the intratumoral TCR repertoire in human cancers. Nature medicine **2019**;25:89-94
37. Simoni Y, Becht E, Fehlings M, Loh CY, Koo SL, Teng KWW*, et al.* Bystander CD8(+) T cells are abundant and phenotypically distinct in human tumour infiltrates. Nature **2018**;557:575-9
38. June CH, Sadelain M. Chimeric Antigen Receptor Therapy. The New England journal of medicine **2018**;379:64-73
39. Ahmed N, Brawley VS, Hegde M, Robertson C, Ghazi A, Gerken C*, et al.* Human Epidermal Growth Factor Receptor 2 (HER2) -Specific Chimeric Antigen Receptor-Modified T Cells for the Immunotherapy of HER2-Positive Sarcoma. Journal of clinical oncology : official journal of the American Society of Clinical Oncology **2015**;33:1688-96
40. Moon EK, Wang LC, Dolfi DV, Wilson CB, Ranganathan R, Sun J*, et al.* Multifactorial T-cell hypofunction that is reversible can limit the efficacy of chimeric antigen receptor-transduced human T cells in solid tumors. Clinical cancer research : an official journal of the American Association for Cancer Research **2014**;20:4262-73
41. O'Rourke DM, Nasrallah MP, Desai A, Melenhorst JJ, Mansfield K, Morrissette JJD*, et al.* A single dose of peripherally infused EGFRvIII-directed CAR T cells mediates antigen loss and induces adaptive resistance in patients with recurrent glioblastoma. Science translational medicine **2017**;9
42. Chen J, Lopez-Moyado IF, Seo H, Lio CJ, Hempleman LJ, Sekiya T*, et al.* NR4A transcription factors limit CAR T cell function in solid tumours. Nature **2019**;567:530-4
43. Proietti M, Cornacchione V, Rezzonico Jost T, Romagnani A, Faliti CE, Perruzza L*, et al.* ATP-gated ionotropic P2X7 receptor controls follicular T helper cell numbers in Peyer's patches to promote host-microbiota mutualism. Immunity **2014**;41:789-801
44. Soto R, Petersen C, Novis CL, Kubinak JL, Bell R, Stephens WZ*, et al.* Microbiota promotes systemic T-cell survival through suppression of an apoptotic factor. Proceedings of the National Academy of Sciences of the United States of America **2017**;114:5497-502
45. Stark R, Wesselink TH, Behr FM, Kragten NAM, Arens R, Koch-Nolte F*, et al.* T RM maintenance is regulated by tissue damage via P2RX7. Science immunology **2018**;3
46. Borges da Silva H, Beura LK, Wang H, Hanse EA, Gore R, Scott MC*, et al.* The purinergic receptor P2RX7 directs metabolic fitness of long-lived memory CD8(+) T cells. Nature **2018**;559:264-8
47. Adinolfi E, Capece M, Franceschini A, Falzoni S, Giuliani AL, Rotondo A*, et al.* Accelerated tumor progression in mice lacking the ATP receptor P2X7. Cancer research **2015**;75:635-44
48. Irizarry RA, Hobbs B, Collin F, Beazer-Barclay YD, Antonellis KJ, Scherf U*, et al.* Exploration, normalization, and summaries of high density oligonucleotide array probe level data. Biostatistics **2003**;4:249-64
49. Tusher VG, Tibshirani R, Chu G. Significance analysis of microarrays applied to the ionizing radiation response. Proceedings of the National Academy of Sciences of the United States of America **2001**;98:5116-21

50. Adorno M, Cordenonsi M, Montagner M, Dupont S, Wong C, Hann B*, et al.* A Mutant-p53/Smad complex opposes p63 to empower TGFbeta-induced metastasis. Cell **2009**;137:87-98
51. Rustighi A, Zannini A, Tiberi L, Sommaggio R, Piazza S, Sorrentino G*, et al.* Prolyl-isomerase Pin1 controls normal and cancer stem cells of the breast. EMBO molecular medicine **2014**;6:99-119
52. Cordenonsi M, Zanconato F, Azzolin L, Forcato M, Rosato A, Frasson C*, et al.* The Hippo transducer TAZ confers cancer stem cell-related traits on breast cancer cells. Cell **2011**;147:759-72
53. Baragetti A, Norata GD, Sarcina C, Rastelli F, Grigore L, Garlaschelli K*, et al.* High density lipoprotein cholesterol levels are an independent predictor of the progression of chronic kidney disease. Journal of internal medicine **2013**;274:252-62
54. Norata GD, Garlaschelli K, Ongari M, Raselli S, Grigore L, Catapano AL. Effects of fractalkine receptor variants on common carotid artery intima-media thickness. Stroke **2006**;37:1558-61
55. Todd JN, Poon W, Lyssenko V, Groop L, Nichols B, Wilmot M*, et al.* Variation in Glucose Homeostasis Traits Associated With P2RX7 Polymorphisms in Mice and Humans. The Journal of clinical endocrinology and metabolism **2015**;100:E688-96
56. Baragetti A, Palmen J, Garlaschelli K, Grigore L, Pellegatta F, Tragni E*, et al.* Telomere shortening over 6 years is associated with increased subclinical carotid vascular damage and worse cardiovascular prognosis in the general population. Journal of internal medicine **2015**;277:478-87

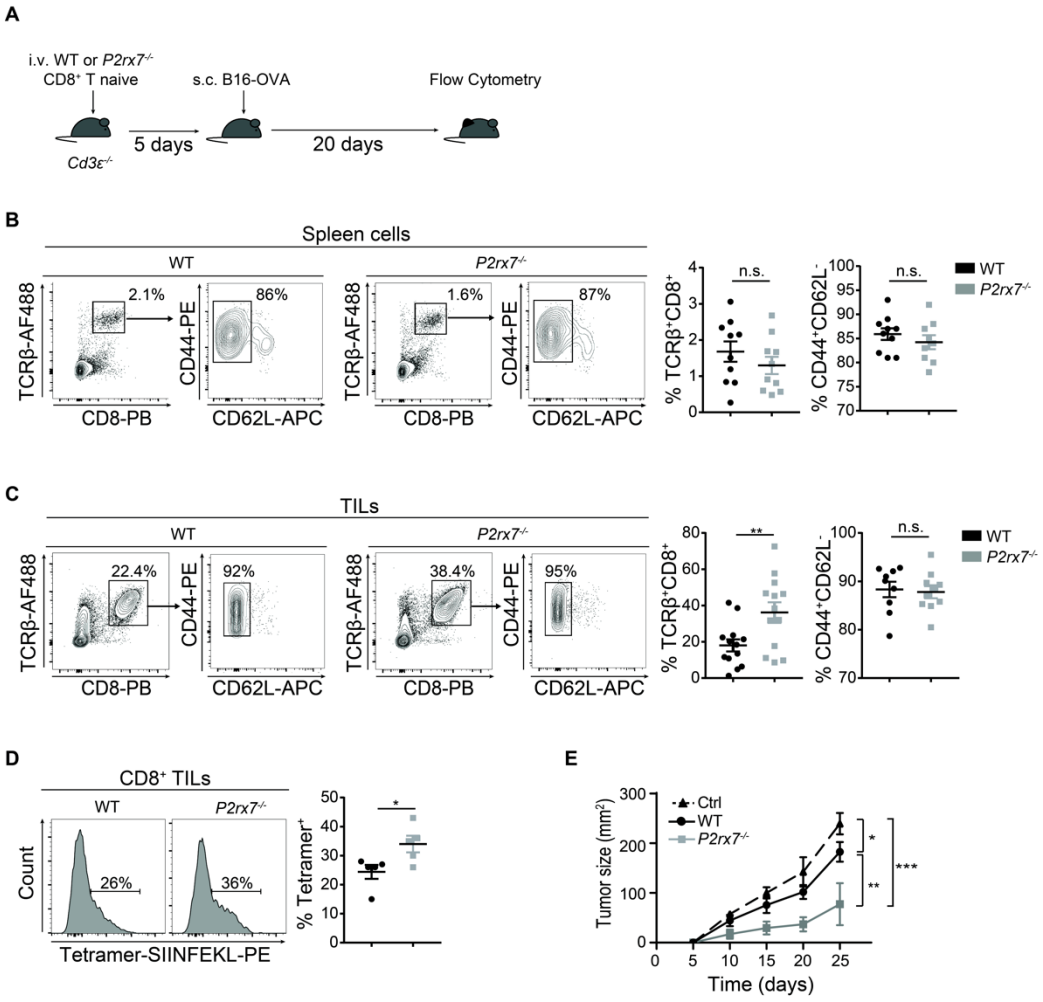

Fig.1. Enhanced accumulation and control of tumor growth by *P2rx7*$^{-/-}$ CD8$^+$ TILs.(**A-E**) *Cd3ε*$^{-/-}$ mice were adoptively transferred with WT or *P2rx7*$^{-/-}$ naive CD8$^+$ T cells, engrafted with B16-OVA cells and sacrificed as indicated. (**A**) Experimental design. (**B-C**) Representative flow cytometry plots and statistical analysis (mean ± SEM) for CD8$^+$ TCRβ$^+$ cells within (**B**) splenocytes (n=10) and (**C**) TILs (n=13), with distribution for CD44 and CD62L expression. Percentages of positive cells in each gate are shown. Data from three independent experiments. (**D**) Flow cytometry histograms and statistical analysis (mean ± SEM) for tetramer positive TILs gated as CD8$^+$ TCRβ$^+$ cells (n=5). Data from one experiment representative of three. Percentages of positive cells are shown. (**E**) Kinetics of tumor growth. Data from one experiment representative of two (n=5). Two-tailed Mann-Whitney U test for the comparison of two groups or two-way ANOVA for comparison of tumor size was used. n.s. not significant, * $p<0.05$, ** $p<0.01$, *** $p<0,001$.

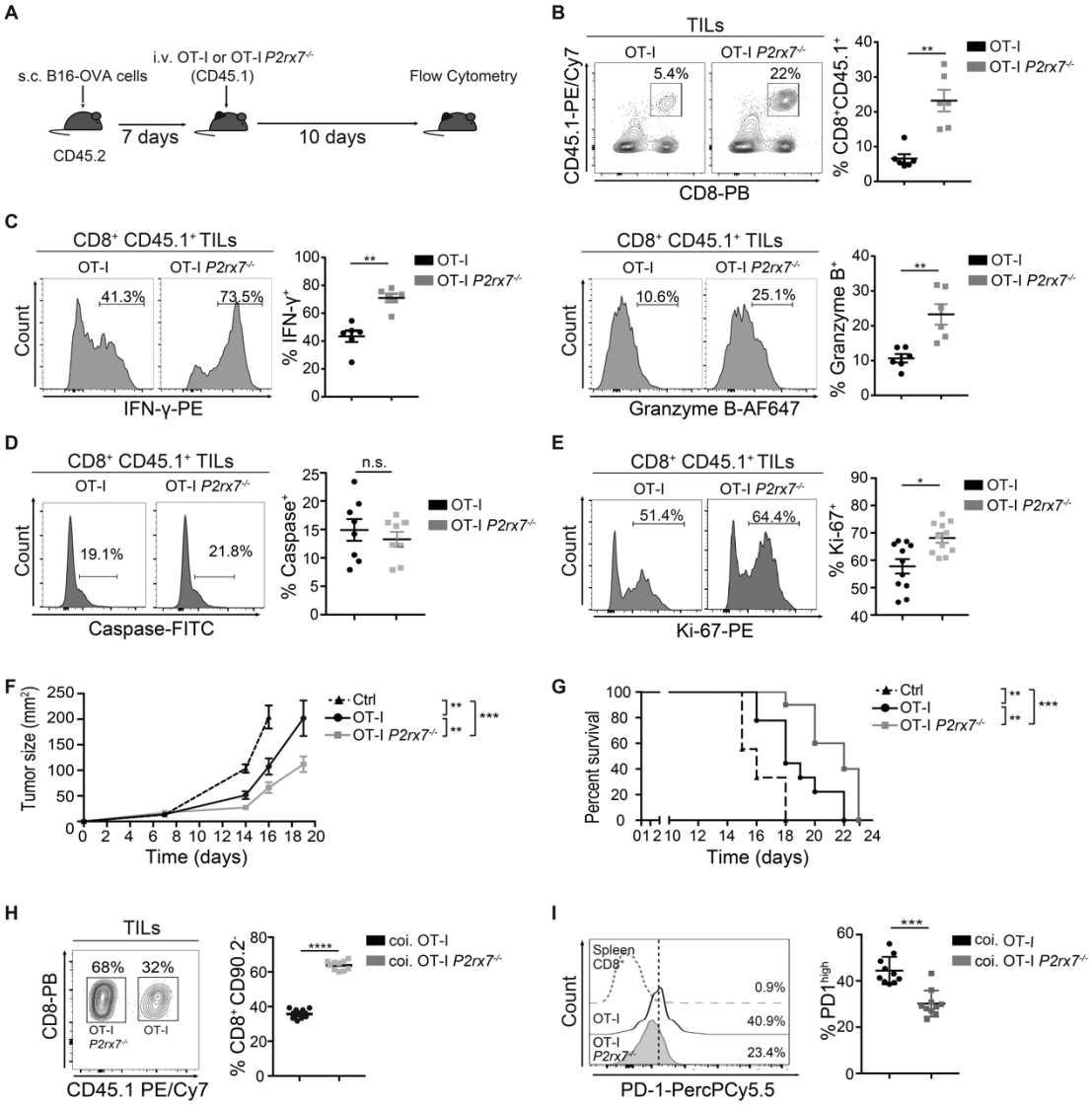

Fig.2. Enhanced control of B16-OVA tumor growth and mice survival by *P2rx7*$^{-/-}$ OT-I TILs. (**A-G**) CD45.2^{+} mice were engrafted with B16-OVA cells and injected with CD45.1^{+}CD8^{+} *Rag1*$^{-/-}$*/P2rx7*$^{+/+}$ (OT-I) or *Rag1*$^{-/-}$*/P2rx7*$^{-/-}$ (OT-I *P2rx7*$^{-/-}$) OT-I cells, initially primed *in vitro*. (**A**) Experimental design. (**B-C**) Representative flow cytometry plots and statistical analysis (mean ± SEM) for CD45.1^{+}CD8^{+} TILs (**B**), IFN-γ (left) and Granzyme B (right) secretion in CD45.1^{+}CD8^{+} TILs (**C**) (n=6). (**D-E**) Flow cytometry histograms and statistical analysis (mean ± SEM) for cells positive for activated caspase (n=8) (**D**) and Ki-67 (n=11) (**E**) within CD45.1^{+}CD8^{+} TILs. Percentages of positive cells in the indicated gates are shown. Data from two independent experiments. (**F**) Kinetics of tumor growth and (**G**) Kaplan-Meier survival plot. One experiment representative of two (n=9 for each group). (**H-I**) Tumor bearing CD45.2^{+}CD90.2^{+} mice were co-injected with CD45.1^{+}CD90.1^{+} *Rag1*$^{-/-}$*/P2rx7*$^{+/+}$ (OT-I) and CD45.2^{+}CD90.1^{+} *Rag1*$^{-/-}$*/P2rx7*$^{-/-}$ (OT-I *P2rx7*$^{-/-}$) OT-I cells. Representative flow cytometry plot and statistical analysis (mean ± SEM) for CD90.2^{-}CD45.1^{+}CD8^{+} (OT-I) or CD90.2^{-}CD45.1^{-}CD8^{+} (OT-I *P2rx7*$^{-/-}$) TILs (**H**) and PD-1^{hi} cells within CD90.2^{-}CD45.1^{+}CD8^{+} (OT-I) or CD90.2^{-}CD45.2^{+}CD8^{+} (OT-I *P2rx7*$^{-/-}$) TILs, and CD8^{+}TCRβ^{+} cells from spleen (Spleen) (**I**). Percentages of positive cells in each gate are shown. Data from 2 independent experiments (n=10). Two-tailed Mann-Whitney U test for the comparison of two groups or two-way ANOVA for comparison of tumor size was used. Mantel-Cox test for analysis of survival. n.s. not significant, * p<0.05, ** p<0.01, *** p<0,001, **** p<0,0001.

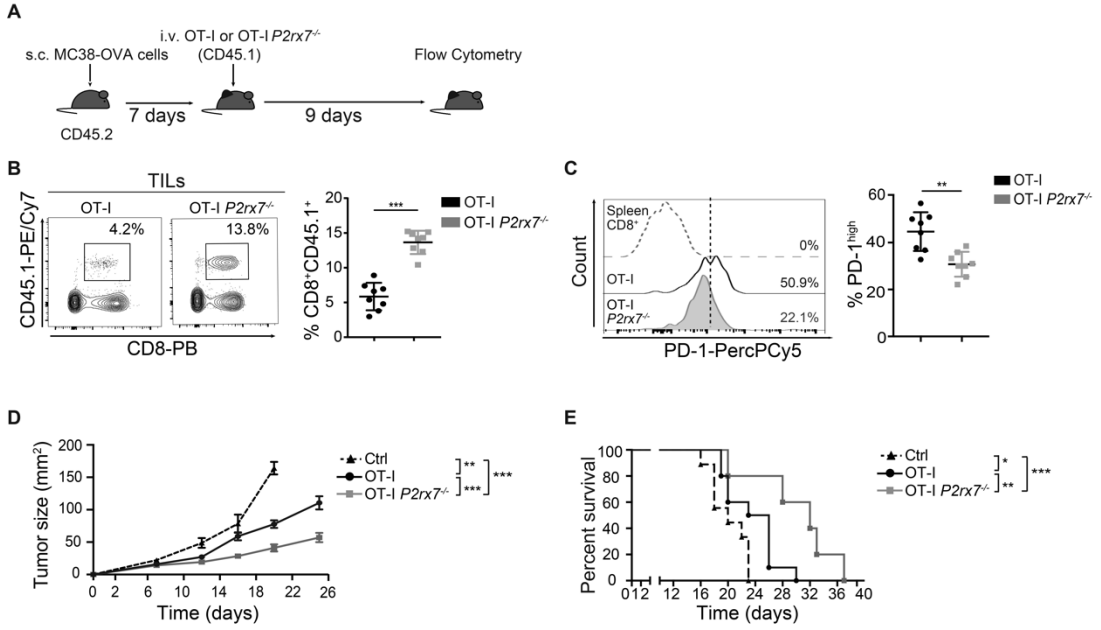

Fig.3. Enhanced control of MC38-OVA tumor growth and mice survival by *P2rx7*$^{-/-}$ OT-I TILs. (**A-E**) CD45.2^{+} mice were engrafted with MC38-OVA cells and injected with CD45.1^{+}CD8^{+} *Rag1*$^{-/-}$/*P2rx7*$^{+/+}$ (OT-I) or *Rag1*$^{-/-}$/*P2rx7*$^{-/-}$ (OT-I *P2rx7*$^{-/-}$) OT-I cells, initially primed *in vitro*. (**A**) Experimental design. (**B**) Representative flow cytometry plots and statistical analysis (mean ± SEM) for CD45.1^{+}CD8^{+} TILs. (**C**) Flow cytometry histograms and statistical analysis (mean ± SEM) for PD-1^{hi} cells within OT-I and OT-I *P2rx7*$^{-/-}$ TILs, and CD8^{+}TCRβ^{+} cells from spleen (Spleen). Percentages of positive cells in each gate are shown. Data from 3 independent experiments (n=8). (**D**) Kinetics of tumor growth and (**E**) Kaplan-Meier survival plot. One experiment representative of two, n=9 mice for each group. Two-tailed Mann-Whitney U test for the comparison of two groups or two-way ANOVA for comparison of tumor size was used. Mantel-Cox test for analysis of survival. * p<0.05, ** p<0.01, *** p<0,001, **** p<0,0001

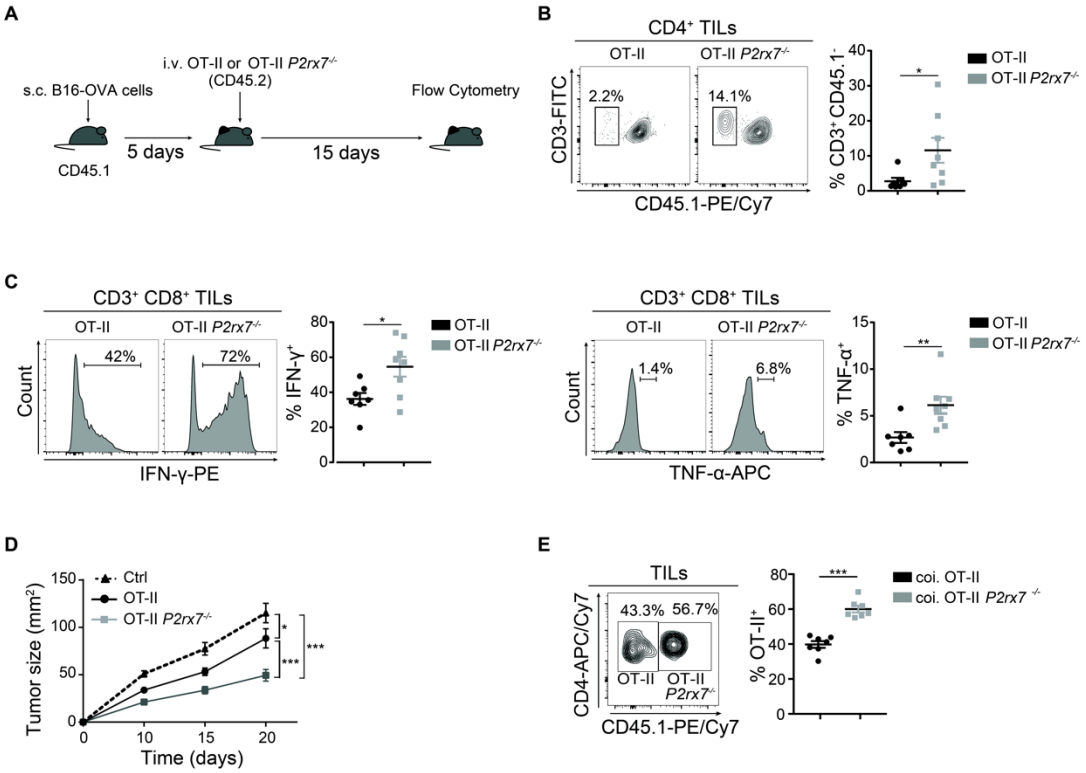

Fig.4. P2X7 activity limits CD4$^+$ TILs expansion in B16 melanoma. (**A-D**) CD45.1$^+$ mice were engrafted with B16-OVA cells and injected with CD45.2$^+$CD4$^+$ *Rag1*$^{-/-}$*/P2rx7*$^{+/+}$ (OT-II) or *Rag1*$^{-/-}$*/P2rx7*$^{-/-}$ (OT-II *P2rx7*$^{-/-}$) OT-II cells, initially primed *in vitro*. (**A**) Experimental design. (**B**) Representative flow cytometry plots and statistical analysis (mean ± SEM) for CD3$^+$CD45.1$^-$ cells gated on CD4$^+$ TILs. (**C**) Flow cytometry histograms and statistical analysis (mean ± SEM) for IFN-γ (left) and TNF-α (right) secretion in CD3$^+$CD8$^+$ TILs. Percentages of positive cells in the indicated gates are shown. (**D**) Kinetics of tumor growth. Data from two independent experiments (n=8). (**E**) Tumor bearing CD45.2$^+$ mice were co-injected with CD45.2$^+$CD4$^+$Vα2Vβ5.1/5.2$^+$ *Rag1*$^{-/-}$*/P2rx7*$^{+/+}$ (OT-II) and CD45.1$^+$CD4$^+$Vα2Vβ5.1/5.2$^+$ *Rag1*$^{-/-}$*/P2rx7*$^{-/-}$ (OT-II *P2rx7*$^{-/-}$) OT-II cells. Representative flow cytometry plots of CD45.1 and CD4 staining on gated Vα2Vβ5.1/5.2$^+$ cells and statistical analysis of OT-II and OT-II *P2rx7*$^{-/-}$ TILs (mean ± SEM). Data from two independent experiments (n=7). Two-tailed Mann-Whitney U test for the comparison of two groups or two-way ANOVA for comparison of tumor size was used. * p<0.05, ** p<0.01, *** p<0,001.

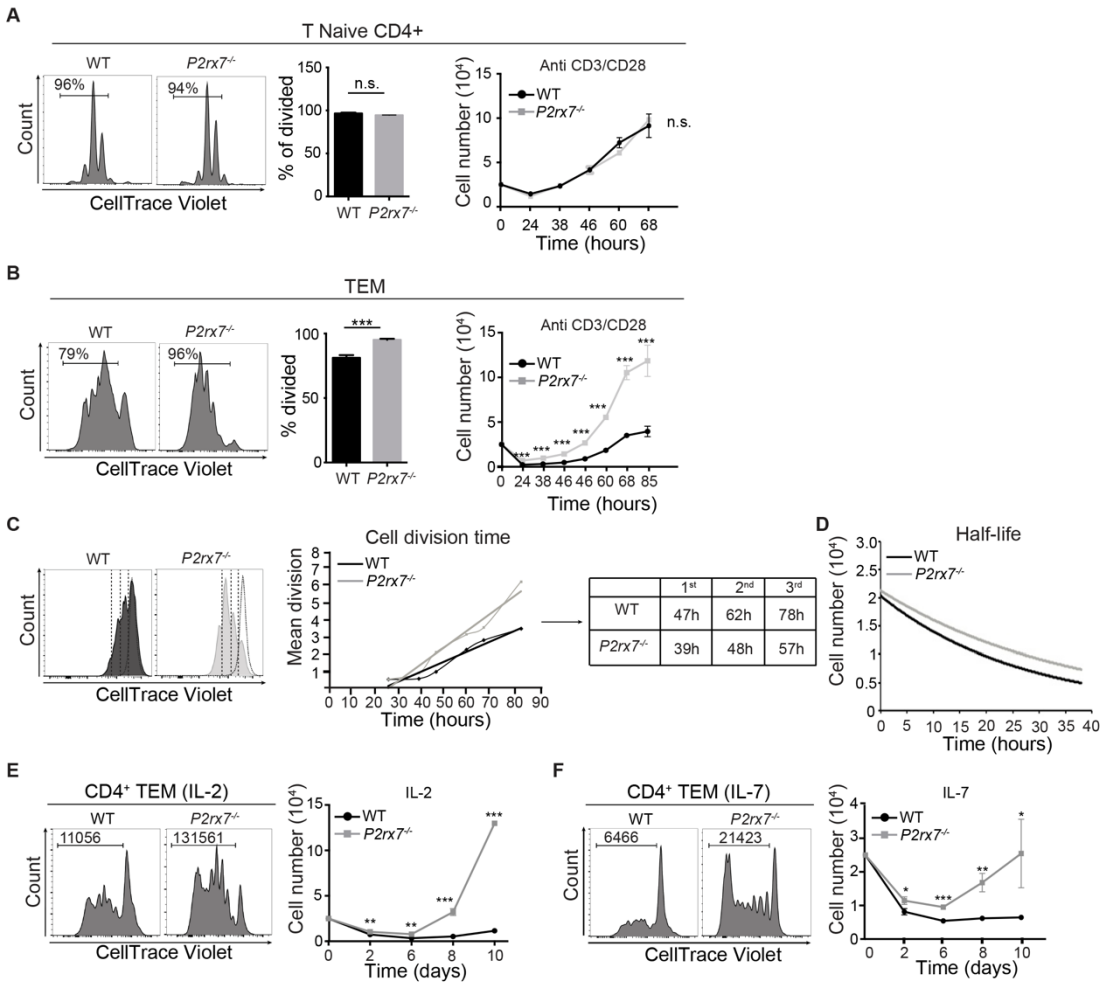

Fig.5. P2X7 activity inhibits proliferation of mouse TEM but not naïve cells. (**A-B**) Mouse WT and *P2rx7*$^{-/-}$ CD4^{+} T naïve or TEM cells were stimulated with anti-CD3/CD28 antibodies. Representative CellTrace Violet dilution in WT and *P2rx7*$^{-/-}$ T naïve (**A**) and TEM (**B**) cells after 72 h stimulation and statistical analysis of divided cells. Numbers in histogram plots indicate percentages of divided cells. The graph on the right shows cell recoveries at different time points after stimulation. (**C**) Linear regression analysis of mean division number against harvest time. The table on the right shows the time taken for WT and *P2rx7*$^{-/-}$ TEM cells to enter into each subsequent division. (**D**) Overtime analyses of TEM cells half-life. (**E-F**) Representative CellTrace Violet dilution in flow cytometry of WT and *P2rx7*$^{-/-}$ TEM cells after 10 days stimulation in IL-2 (**E**) or IL-7 (**F**). The absolute number of dividing cells is reported in the left corner of the histogram plot. The graph on the right shows cell recoveries at different time points after stimulation. Data are from three independent experiments with five pooled mice per sample. Two-tailed Mann-Whitney U test for the comparison of two groups or Kruskall-Wallis test for the comparison of more than two groups. n.s. not significant, * $p<0.05$, ** $p<0.01$ *** $p<0,001$.

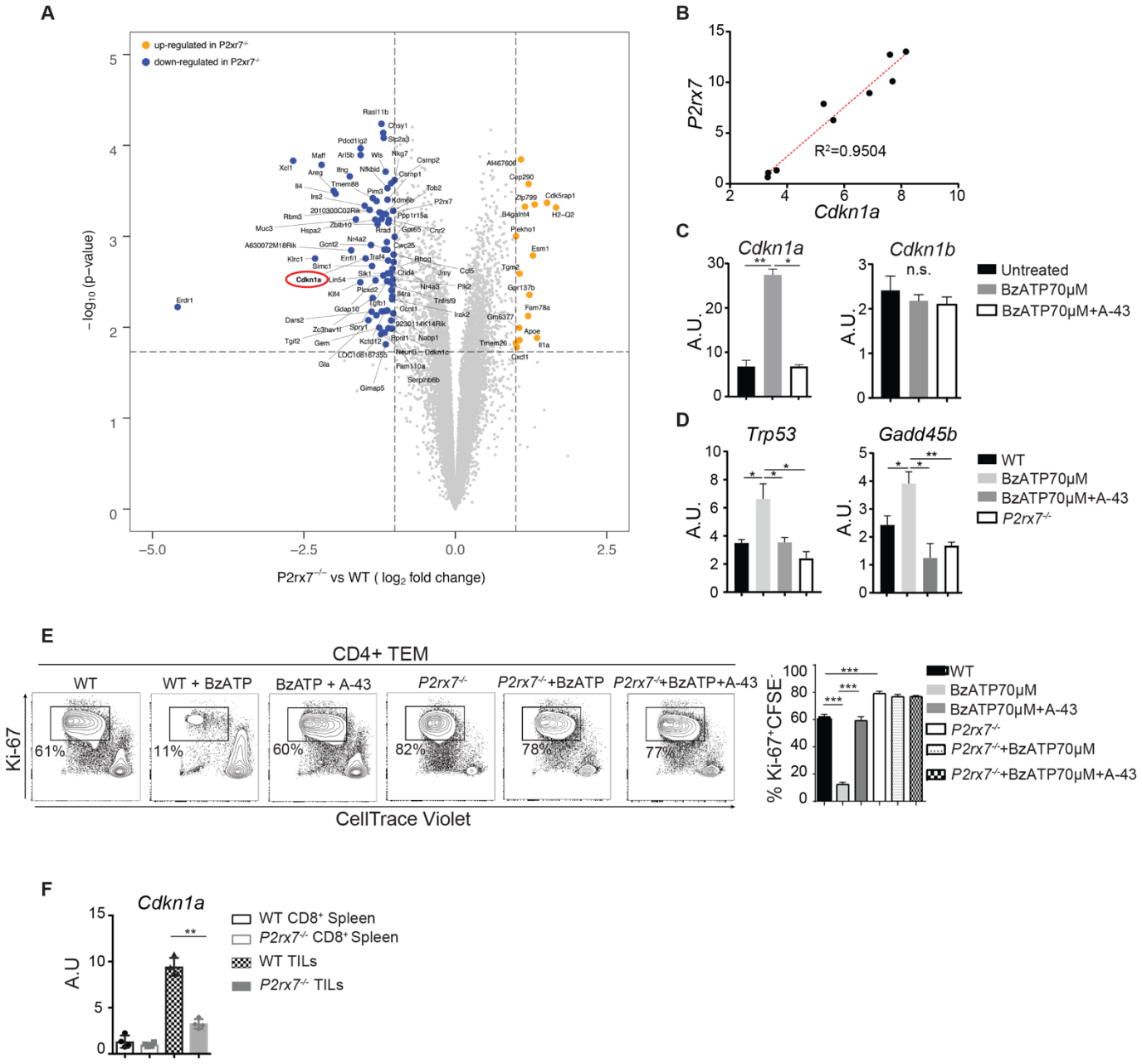

Fig.6. P2X7 stimulation in TEM cells induces cell cycle arrest. (**A**) Volcano plot showing the most significantly differentially expressed genes in the comparison of *ex vivo* purified CD4$^+$ TEM cells from *P2rx7*$^{-/-}$ (n = 3 independent samples) and WT (n = 3 independent samples) mice. Blue and yellow dots indicate down- and up-regulated genes in *ex vivo P2rx7*$^{-/-}$ CD4$^+$ TEM cells (absolute fold change ≥2 and FDR ≤5%; table S3). P-values on the y axis were derived from Significance Analysis of Microarray (see Methods). Unadjusted P values are shown. (**B**) Correlation between *Cdkn1a* and *P2rx7* transcript levels in mouse CD4$^+$ T cells at different times after stimulation with anti-CD3 and anti-CD28 antibodies. (**C-D**) WT and *P2rx7*$^{-/-}$ CD4$^+$ TEM cells were stimulated *in vitro* with BzATP for 24 h in the presence of the P2X7 inhibitor A-438079 (A-43) 50 μM where indicated. Data are from three independent experiments with five pooled mice per sample. (**C**) qRT-PCR of *Cdkn1a* (left) and *Cdkn1b* (right) transcripts. (**D**) qRT-PCR of *Trp53* (left) and *Gadd45b* (right) transcripts. (**E**) WT and *P2rx7*$^{-/-}$ CD4$^+$ TEM cells were stimulated with anti-CD3/CD28 antibodies for 72 h in presence of BzATP and A-43 50 μM where indicated. Data are from three independent experiments with five pooled mice

per sample. Representative flow cytometry plots for CellTrace Violet dilution and Ki-67 staining. Percentages of cycling Ki-67^{+} cells in the displayed gate and relative statistics are shown. (**F**) qRT-PCR of *Cdkn1a* in CD8^{+} splenocytes and TILs from *Cd3ε*$^{-/-}$ mice adoptively transferred with WT or *P2rx7*$^{-/-}$ CD8^{+} T naive cells and subsequently engrafted with B16-OVA cells (n=4). A.U., Arbitrary Unit. Statistical analysis shows means ± SEM. Two-tailed Mann-Whitney U test for the comparison of two groups or Kruskall-Wallis test for the comparison of more than two groups. n.s. not significant, * $p<0.05$, ** $p<0.01$ *** $p<0,001$.

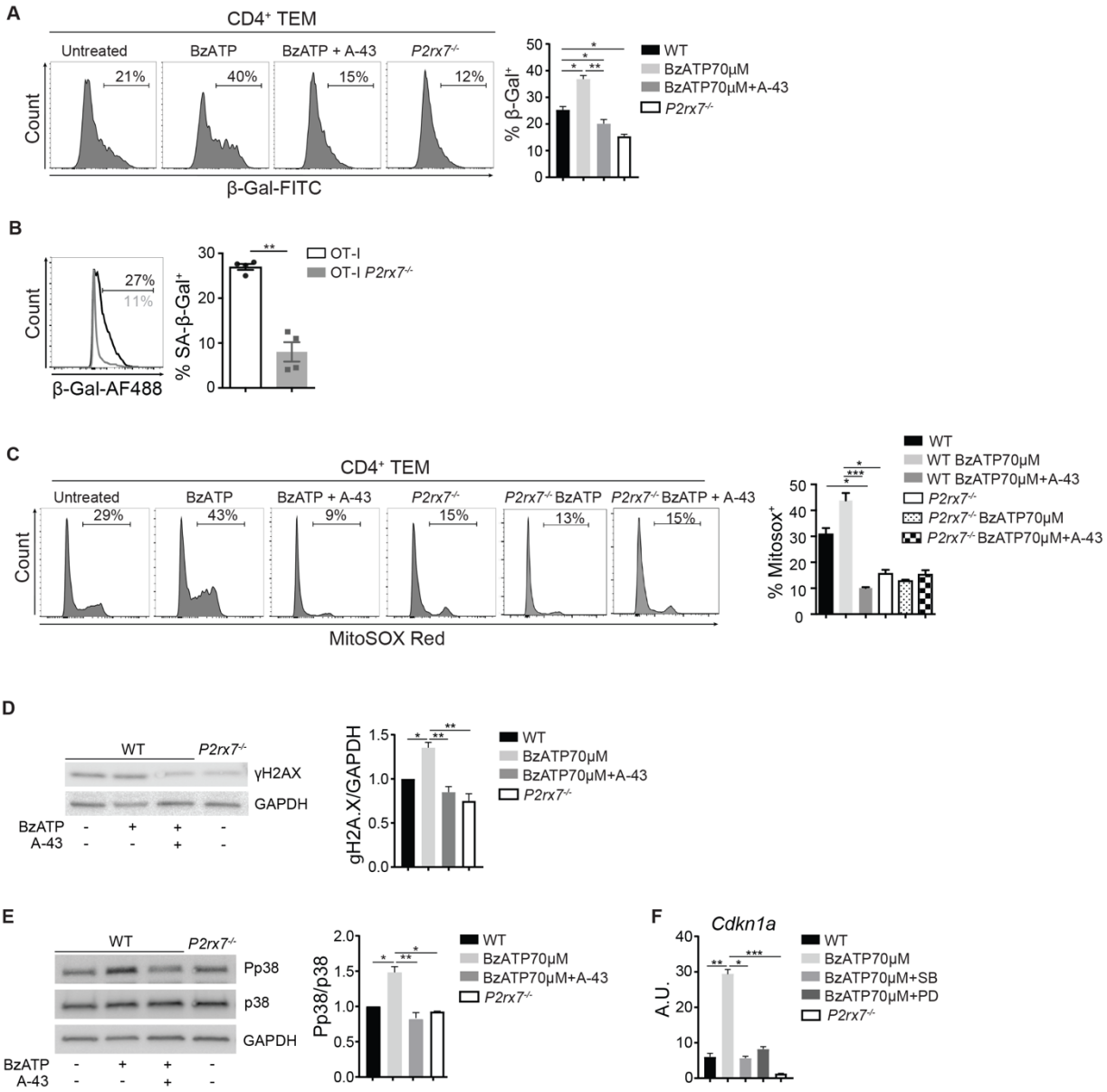

Fig. 7. P2X7 stimulation in TEM cells leads to premature senescence. (**A**) Representative flow cytometry histograms and statistical analysis for SA β-galactosidase staining on *ex vivo* CD4$^+$ TEM cells stimulated with anti-CD3/CD28 antibodies for 72 h in the presence of the indicated treatments. Percentages of positive cells are shown (n=3). (**B**) Representative flow cytometry histograms and statistical analysis for SA β-galactosidase staining of *Rag1*$^{-/-}$*/P2rx7*$^{+/+}$ (OT-I) and *Rag1*$^{-/-}$*/P2rx7*$^{-/-}$ (OT-I *P2rx7*$^{-/-}$) TILs from B16-OVA tumor bearing WT mice. Percentages of positive cells are shown (n=4). (**C-E**) *Ex vivo* CD4$^+$ TEM cells were stimulated with anti-CD3/CD28 antibodies for 72 h in the presence of the indicated treatments. Where indicated, cells were pretreated with A-438079 (A-43) 50 μM for 30 min. Data are from three independent experiments with five pooled mice per sample. (**C**) Representative flow cytometry histograms and statistical analysis of WT and *P2rx7*$^{-/-}$ CD4$^+$ TEM cells labelled with MitoSOX Red. Numbers in graphs indicate the percentage of positive cells. (**D**) Western blot on protein extracts from WT and *P2rx7*$^{-/-}$ CD4$^+$ TEM cells. Membranes were probed for histone H2AX phosphorylated at serine 139 (γ-H2Ax) and GAPDH. Histograms show the statistical analysis of densitometric values of γ-H2Ax normalized on GADPH expression. (**E**) Western blot for p38 MAPK phosphorylation at

Thr180/Tyr182 (Pp38), total p38 protein and GAPDH. Histograms show the statistical analysis of densitometric values of Pp38 normalized on total p38. (**F**) qRT-PCR of *Cdkn1a* transcript. WT and *P2rx7*$^{-/-}$ CD4^{+} TEM cells were stimulated *in vitro* with BzATP for 24 h in the presence of the p38 MAPK inhibitors SB-239063 (SB) 5 µM or PD-169316 (PD) 5 µM where indicated. Data are from three independent experiments with five pooled mice per sample. A.U., Arbitrary Unit. Statistical analysis shows means ± SEM. Two-tailed Mann-Whitney U test for the comparison of two groups or Kruskall-Wallis test for the comparison of more than two groups. n.s. not significant, * $p<0.05$, ** $p<0.01$ *** $p<0,001$.

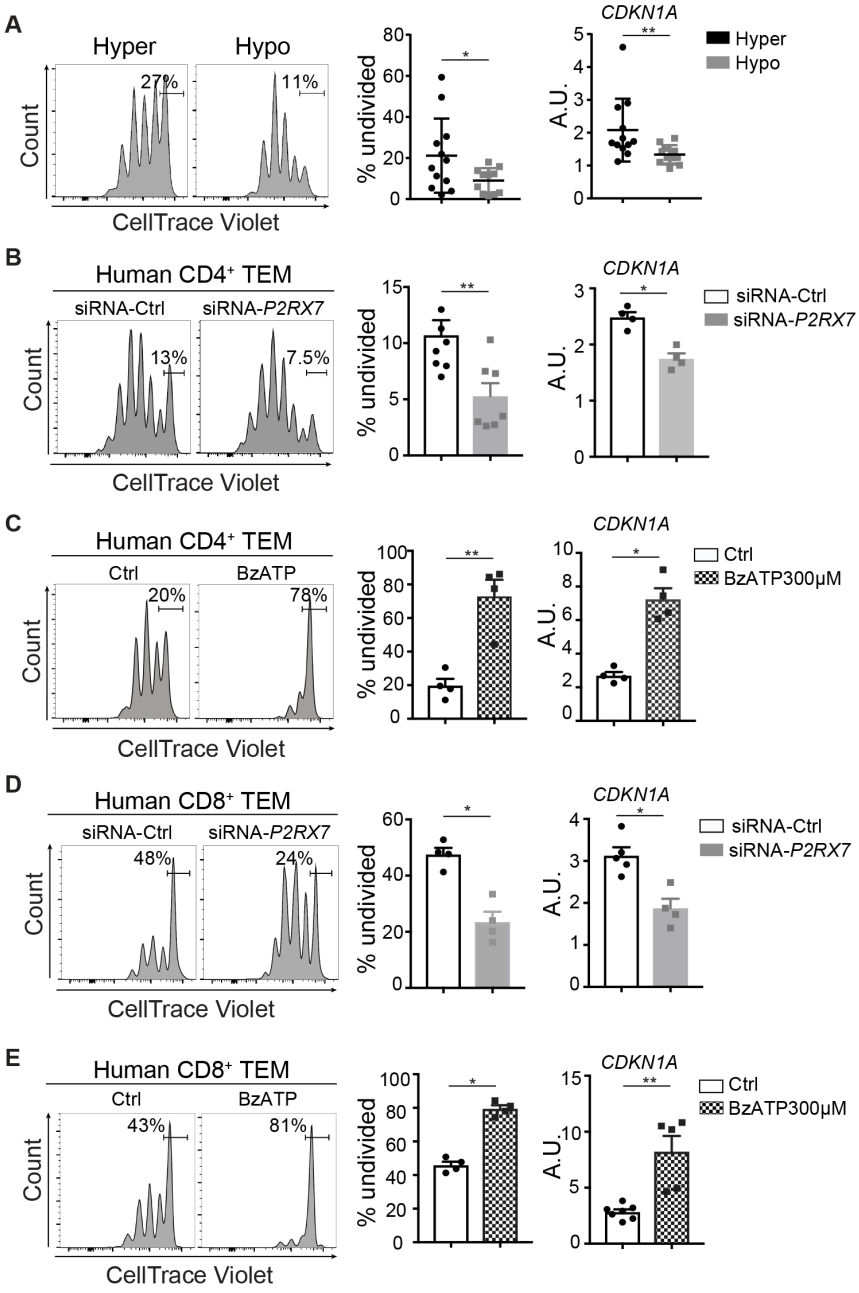

Fig.8. P2X7 activity controls *CDKN1A* transcription and proliferation in human TEM cells. (**A**) TEM cells from human subjects expressing the *P2RX7* hypermorphic (hyper) (n=12) or hypomorphic (hypo) (n=11) gene variant were stimulated with anti-CD3/CD28 antibodies for 72 h. Left: representative histograms of CellTrace Violet dilution and statistical analysis of undivided cells. Numbers in the histogram plots represent the percentage of undivided cells. Right: qRT-PCR for *CDKN1A* transcript on *ex vivo* TEM cells from the same subjects. (**B,D**) Left: representative CellTrace Violet dilution in human $CD4^+$ (**B**) or $CD8^+$ (**D**) TEM cells transfected with siRNA-Ctrl or siRNA-*P2RX7* and stimulated with anti-CD3/CD28 antibodies for 96 h. Numbers in the plots represent the percentage of undivided cells. Right: qRT-PCR for *CDKN1A* transcript on the same cells. (**C,E**) Left: representative CellTrace Violet dilution in $CD4^+$ (**C**) and $CD8^+$ (**E**) TEM cells stimulated with anti-CD3/CD28 antibodies for 96 h either without (Ctrl) or with BzATP 300 µM and statistical analysis of undivided cells. Numbers in the plots represent the percentage of undivided cells. Right: qRT-PCR for *CDKN1A*

transcript on same cells. The two experimental groups in panels B-E were generated from 4 to 7 independent donors and mean ± SEM are shown. A.U., Arbitrary Unit. Two-tailed Mann-Whitney U test for the comparison of two groups or Kruskall-Wallis test for the comparison of more than two groups. In panel A, samples are normally distributed and Student's unpaired t test was used. * $p<0.05$, ** $p<0.01$.